NASA/CR-2007-214866

A Supersonic Argon/Air Coaxial Jet Experiment for Computational Fluid Dynamics Code Validation

Chandler W. Clifton and Andrew D. Cutler
The George Washington University, Newport News, Virginia

April 2007

Since its founding, NASA has been dedicated to the advancement of aeronautics and space science. The NASA Scientific and Technical Information (STI) Program Office plays a key part in helping NASA maintain this important role.

The NASA STI Program Office is operated by Langley Research Center, the lead center for NASA's scientific and technical information. The NASA STI Program Office provides access to the NASA STI Database, the largest collection of aeronautical and space science STI in the world. The Program Office is also NASA's institutional mechanism for disseminating the results of its research and development activities. These results are published by NASA in the NASA STI Report Series, which includes the following report types:

- TECHNICAL PUBLICATION. Reports of completed research or a major significant phase of research that present the results of NASA programs and include extensive data or theoretical analysis. Includes compilations of significant scientific and technical data and information deemed to be of continuing reference value. NASA counterpart of peer-reviewed formal professional papers, but having less stringent limitations on manuscript length and extent of graphic presentations.

- TECHNICAL MEMORANDUM. Scientific and technical findings that are preliminary or of specialized interest, e.g., quick release reports, working papers, and bibliographies that contain minimal annotation. Does not contain extensive analysis.

- CONTRACTOR REPORT. Scientific and technical findings by NASA-sponsored contractors and grantees.

- CONFERENCE PUBLICATION. Collected papers from scientific and technical conferences, symposia, seminars, or other meetings sponsored or co-sponsored by NASA.

- SPECIAL PUBLICATION. Scientific, technical, or historical information from NASA programs, projects, and missions, often concerned with subjects having substantial public interest.

- TECHNICAL TRANSLATION. English-language translations of foreign scientific and technical material pertinent to NASA's mission.

Specialized services that complement the STI Program Office's diverse offerings include creating custom thesauri, building customized databases, organizing and publishing research results ... even providing videos.

For more information about the NASA STI Program Office, see the following:

- Access the NASA STI Program Home Page at *http://www.sti.nasa.gov*

- E-mail your question via the Internet to help@sti.nasa.gov

- Fax your question to the NASA STI Help Desk at (301) 621-0134

- Phone the NASA STI Help Desk at (301) 621-0390

- Write to:
  NASA STI Help Desk
  NASA Center for AeroSpace Information
  7115 Standard Drive
  Hanover, MD 21076-1320

A Supersonic Argon/Air Coaxial Jet Experiment for Computational Fluid Dynamics Code Validation

Chandler W. Clifton and Andrew D. Cutler
The George Washington University, Newport News, Virginia

National Aeronautics and
Space Administration

Langley Research Center
Hampton, Virginia 23681-2199

April 2007

ABSTRACT

A non-reacting experiment is described in which data has been acquired for the validation of CFD codes used to design high-speed air-breathing engines. A coaxial jet-nozzle has been designed to produce pressure-matched exit flows of Mach 1.8 at 1 atm in both a center jet of argon and a coflow jet of air, creating a supersonic, incompressible mixing layer. The flowfield was surveyed using total temperature, gas composition, and Pitot probes. The data set was compared to CFD code predictions made using Vulcan, a structured grid Navier-Stokes code, as well as to data from a previous experiment in which a He-O_2 mixture was used instead of argon in the center jet of the same coaxial jet assembly.

Comparison of experimental data from the argon flowfield and its computational prediction shows that the CFD produces an accurate solution for most of the measured flowfield. However, the CFD prediction deviates from the experimental data in the region downstream of $x/D = 4$, underpredicting the mixing-layer growth rate.

TABLE OF CONTENTS

LIST OF FIGURES

LIST OF TABLES

LIST OF MAJOR SYMBOLS

C	Courant-Friedrichs-Lewy number
D	Coaxial jet nozzle diameter
χ	Mole fraction
δ	Uncertainty
$\delta'_{vis,0}$	Visual thickness of incompressible mixing layer
$\delta'_{pit,0}$	Measured thickness of incompressible mixing layer
δ'_{pit}	Measured thickness of compressible mixing layer
$\delta_{0.01}$	Radial distance to 1% mole fraction points
$\delta_{0.99}$	Radial distance to 99% mole fraction points
γ	Ratio of specific heats
h	Enthalpy
M	Mach number
M_c	Convective Mach number
μ	Viscosity
Pr_t	Turbulent Prandtl number
P_{amb}	Ambient pressure
P_{pit}	Pitot pressure
$P_{ref,CJ}$	Center-jet nozzle reference pressure
$P_{ref,coflow}$	Coflow nozzle reference pressure
P_{exit}	Nozzle exit pressure
ρ	Density
Sc_t	Turbulent Schmidt number
$T_{ref,coflow}$	Coflow nozzle total temperature
$T_{ref,CJ}$	Center-jet nozzle total temperature
T_{amb}	Ambient temperature
T_t	Total temperature
u	Velocity
Y	Mass fraction
x, y, z	Position coordinates

CHAPTER 1 - INTRODUCTION

1.1 Motivation

Travel into space has been an expensive endeavor since its beginnings and lowering costs associated with a typical launch vehicle has become an important priority. In the effort to provide cheaper access to space, one begins to consider propulsion technologies less consumptive than rockets to achieve the task of attaining orbital flight. Air-breathing propulsion potentially offers significant gross-take-off weight savings compared to rockets because an onboard oxidizer is not required for combustion. The supersonic combustion ramjet (scramjet) is the preferred air-breathing engine for hypersonic flight, and offers a potentially cheaper alternative for high Mach number flight to space as well as for military applications.

One of the most difficult aspects in the design of scramjet engines is that of establishing an efficient supersonic combustion process over a wide range of flight Mach numbers. The fuel injection system and combustor geometry must simultaneously provide sufficient fuel-air mixing and minimal losses. Yet, high flow velocities and the constraint of maintaining reasonable combustor length scales typically yield a combined mixing and combustion time requirement on the order of milliseconds.[1]

Within a supersonic combustion chamber, fuel is injected into the main air stream as high-speed jets. The mixing that occurs between these compressible streams has proven to be difficult to correctly simulate; however, as computational and analytic capabilities have matured, so too have the characterizations of these complex, turbulent flows through the application of Computational Fluid Dynamics (CFD) codes become more accurate and economical. Generally, these codes are only accepted design tools in scenarios for which they have been validated through testing. This has proven particularly true for high-speed engine design since slight variations in the mixing rate predictions can result in large discrepancies in combustor performance. Therefore, it is necessary to collect calibration data in order to validate CFD results, as well as to establish valid ranges of code applicability.

1.2 Background

The need for a better understanding of supersonic mixing led to experiments which examined the effects of compressibility on mixing-layer growth, such as the experiment of Papamoshou and Roshko.[2] The convective Mach number, M_c, has since become a conventional parameter used to characterize mixing-layer growth rate reduction due to mixing-layer compressibility. These earlier experiments were conducted in blowdown or constant flow facilities, limiting the attainable M_c to about 1.5. More recently, experiments have been conducted in facilities capable of creating higher convective Mach numbers. Experiments of Rossmann et al.[3,4] used a shock tunnel to achieve $2<M_c<4$, allowing the examination of mixing-layer growth rates, as well as the physical mechanisms which govern them, at these higher M_c's.

In the previous decade, progress was relatively slow in terms of improving simulations of high-speed mixing flows; however, much effort has been put forth in

recent years to upgrade modeling techniques.[1] Even with continuing increases in computational power, Reynolds-Averaged Navier-Stokes (RANS) models are typically preferable over methods employing higher-order (and hence, more costly computationally) closures, such as large eddy simulation (LES), for modeling high-speed compressible reacting flows. Improving RANS simulation approaches is an ongoing challenge, and enhancements to turbulent transport models are likely to be the most beneficial pursuits in high-speed code development.[1] Of particular interest is the treatment of the turbulent Schmidt and turbulent Prandtl numbers, Sc_t and Pr_t respectively.

$$Pr_t = -\frac{\mu_t}{\overline{\rho h'' u''_j}} \frac{\partial \widetilde{h}}{\partial x_j}, \tag{1.1}$$

$$Sc_t = -\frac{\mu_t}{\overline{\rho Y''_m u''_j}} \frac{\partial \widetilde{Y}_m}{\partial x_j}, \tag{1.2}$$

where μ_t represents the isotropic eddy viscosity, $\overline{\rho}$ represents mean density and h'', u''_j, Y''_m represent mass-weighted fluctuating enthalpy, velocity, and mass fraction of species "m", respectively.[1] The turbulent Prandtl and Schmidt numbers specify the ratios of viscous to thermal diffusion fluxes and viscous to mass diffusion fluxes, respectively. Traditionally, the gradient diffusion hypothesis has been used to model a turbulent transport of scalar properties, often leading to an assumption of constant Pr_t and Sc_t.[1] While it has been noted that generally Pr_t and Sc_t do not vary considerably with respect to each other[5] (the ratio of Pr_t to Sc_t is often ~ 1), it has also been shown that they are not constant values, and are known to significantly influence fluid dynamic processes. A small change in Sc_t can cause engine unstart or flame blowout. Questions have been raised as to the validity in assuming constant Pr_t and Sc_t within the context of the gradient diffusion hypothesis,[6,7,8] and Baurle[1] points out that this assumption does not properly characterize the numerous physical phenomena associated with turbulent mass and heat transfer. Thus, in order to address turbulence/chemistry interactions more accurately, the turbulence model should calculate Pr_t and Sc_t as part of the solution.

Brinckman et al.[8,9,10,11] have been creating turbulent scalar fluctuation models that incorporate variable Pr_t and Sc_t. Previous research involved the development and testing of a two-equation temperature fluctuation model and a two-equation mass fluctuation model for comparison with experimental and LES data sets from non-reacting shear layers, jets, and a simple scramjet injector geometry.[9,10] The primary focus was on the effects of high-Mach number compressibility with respect to turbulent Schmidt and Prandtl number variation. The two equations in each model address the variance and dissipation rate of its respective scalar. Good agreement between the models and data sets was found and an improvement in overall solution accuracy was reported for complex flow geometries. More recently, new two-equation scalar fluctuation models with variable Prandtl and Schmidt numbers have been developed for applications in high-speed reacting flows.[8,11] These models are based on previous research[9,10] and accurately reproduce predictions of non-reacting flows, but are designed to avoid chemical source terms in the transport equations due to the modeling difficulties they cause. These new

models were tested on high-speed non-reacting and reacting flows and both models were found to accurately predict experimental data from these flows. The thermal transport model also captured the effect of compressibility on the turbulent Prandtl number. There was mild improvement in the accuracy of predictions of these jets compared to previous models, but more importantly, these predictions relaxed to the well-posed Sc_t and Pr_t values within the flows without biasing the models to known experimental values.

Comparable progress has been reported[6,7,12,13] by Hassan *et al.* with the similar goal of developing variable Sc_t and Pr_t models. The first tests of a variable-Pr_t, two-equation model compared the code predictions with data from high-speed shock wave/boundary layer interactions.[12] This new formulation resulted in greatly improved accuracy of heat-flux calculations. A parallel model was also developed for calculating variable turbulent Schmidt numbers and applied to non-reacting flows.[7] As in the previously mentioned research, predictions were significantly improved over those from traditional turbulent transport models, and later this new model was broadened to make predictions of a high-speed reacting scenario.[13] Overall, good agreement between computation and experimental results was reported.

In the process of improving the modeling of turbulent transport, Hassan *et al.*[7] and Brinkman *et al.*[11] drew upon experimental data gathered by Cutler *et al.*[14] in which a supersonic compressible coaxial jet was examined for CFD code validation. The center jet consisted of a 95% helium and 5% O_2 mixture (by volume) at $M = 1.8$, and was surrounded by a coflow jet of air at $M = 1.8$. Although the Mach numbers of both streams were 1.8, the helium-mixture velocity was more than twice that of the air due to its lighter molecular weight (and consequent greater speed of sound). The resultant convective Mach number of the mixing layer between these streams was ~ 0.7, consistent with the definition of Papamoshou and Roshko.[2] An experimental (probe rake) survey of the coflow mixture effectively measured Pitot pressure, composition, total temperature, and mixing-layer growth rate, and velocity was measured using the RELIEF technique.[15] As a free jet, the coflow was easily accessible by probes and optical systems. The pressures of the jets were matched at 1 atmosphere. Consequently, the flow development was primarily governed by turbulence as opposed to pressure forces, thus requiring an accurate turbulence model within a CFD code for accurate flowfield predictions. Because the coflow was axisymmetric, a minimal number of measurements were required to completely represent the flow, and similarly, computational CFD costs were reduced.

The fuel used in hypersonic flight is typically either hydrogen or a hydrocarbon. As was done in the previously mentioned experiment,[14] helium is often used in tests to simulate the mixing of hydrogen fuel due to its low molecular weight and inert quality. Although hydrogen offers a relatively high energy release per unit mass, hydrocarbon fuels provide higher energy release per unit volume, making them more practical when payload space is an issue, i.e. military vehicles. Argon is a logical choice to represent non-reacting hydrocarbon fuel mixing due to its heavier-than-air molecular weight as well as its inertness. Also, argon is relatively inexpensive because of its natural abundance. Another useful property is that γ_{argon} (1.67) is different than γ_{air}. The method used to measure gas composition by Cutler *et al.*[14] is based on monitoring the voltage across a hot-film probe, sensitive to both γ and molecular weight (MW) of the mixture, to determine mole fraction.

1.3 Objective

This study expands upon the work of Cutler *et al*.,[14] examining the same geometry while using the same instrumentation, but replacing the helium center jet with a supersonic jet of argon. The use of argon in this study is unique compared to recent experiments of this kind, which typically utilize hydrogen and/or helium as test gases. In this case, the speed of sound of argon is only slightly less than that of air, corresponding to a slightly lower speed center jet as compared to the coflow jet and a convective Mach number of 0.17. As a result, gas compressibility should not play a significant role in reducing the mixing rate of the coflow, as it does in mixing flows of relatively high convective Mach numbers.

The objective of this experiment is to provide data for validation and improvement in modeling of scalar transport phenomena, and the overall enhancement of high-speed mixing CFD codes. In particular, the influence of Sc_t and Pr_t on turbulent mixing in a supersonic flow will be examined without the previously mentioned effects of mixing-layer compressibility. As done in the experiment of Cutler *et al*.,[14] Pitot pressure, gas composition, and total temperature measurements were taken using the same model and facility. The Vulcan CFD code was used as it was by Cutler *et al*.[14] for performing flow calculations with the same grids and turbulence model in which constant, assumed Sc_t and Pr_t are optimized. Comparisons are presented between these results and those previously obtained by Cutler *et al*.[14]

This paper describes the facility and instrumentation used as well as data analysis techniques and operating procedures. Also, results are included and discussed in detail, and finally, conclusions are drawn and presented.

CHAPTER 2 – FACILITY AND MODEL

2.1 Test Facility and Assembly

The coaxial jet assembly is presented in figure 1,[14] where dimensions are in mm. It is axisymmetric and consists of a center body and a concentric outer body. The center body contains a supersonic nozzle for the argon jet, and the gap between the center and outer bodies creates a supersonic nozzle for the coflow air jet. Both nozzles were designed to provide a nominal Mach number of 1.8 at the exit. Screens were installed near the entrance of the center body to make the argon stream uniform and to lower turbulence.[14] The outer body is capped with a conical extension ring, which is normally in place, but can be removed to allow probe access to the center nozzle exit. Three streamlined struts extend from the outer body to provide support for the suspended center body. Below this, the mating flange secures the coaxial jet to the plenum. The sharp corners at the entrance of the coflow nozzle may raise concerns over the effect of separations on the flowfield. However, the large downstream contraction ratio should allay these irregularities.[14]

This experiment was conducted in the Transverse Jet Facility (TJF)[16] at NASA Langley Research center in Room 205 of Building 1221c. The TJF consists of a plenum 40 cm in diameter and 110 cm tall, and is shown in figure 2. The plenum is equipped with flow-conditioning screens.
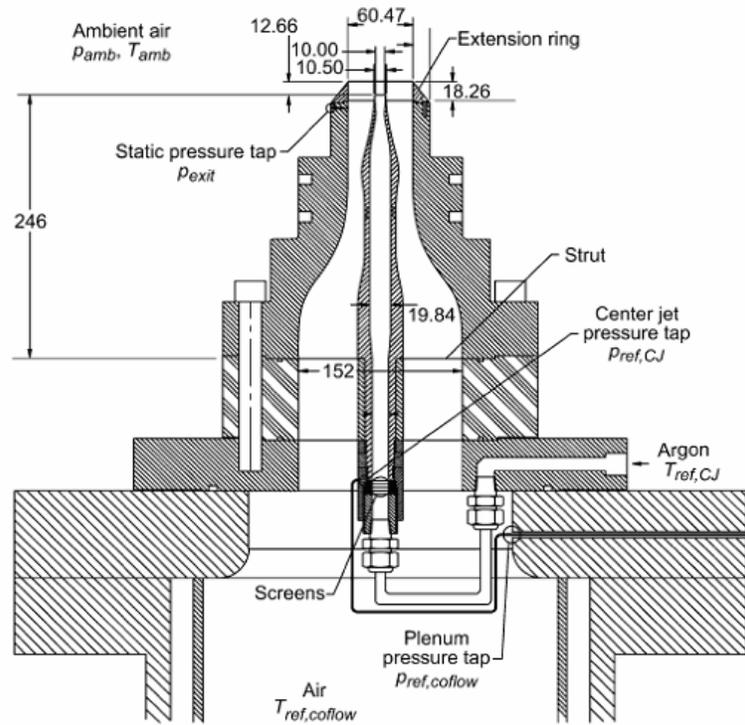
Figure 1   Coaxial jet assembly, from Cutler *et al*.[14]
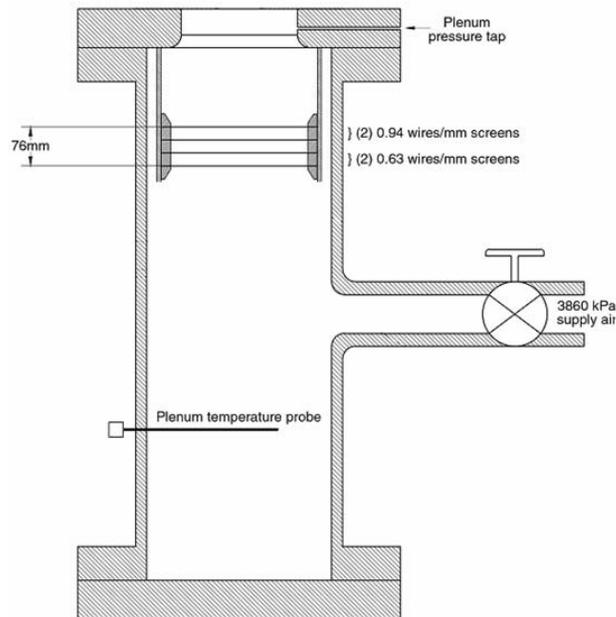
Figure 2   Transverse jet facility, from Doehner[16]

Three pressure taps are located in the nozzle assembly. One is in the center body just downstream of the screens, one is in the coflow body just below the removable ring, and the other is in the facility plenum. Thermocouples are positioned in the gas supply lines. This instrumentation aided in ensuring proper operating conditions and will be discussed further in Chapter 3.

2.2 Operating Conditions

Air was supplied from a central compressor station, allowing a maximum pressure of 600 psi. An orifice plate within this supply restricted the air pressure to a maximum of 100 psi. The plenum pressure upstream of the nozzle was selected to be 84 psi in order for the pressure at the jet exit to be atmospheric. The fuel simulant, argon gas, was supplied from two pallet packs of 16 bottles each that were located outside the building. The bottles were pressurized to 2400 psi, but were regulated to 92 psi before the center nozzle in order to achieve atmospheric pressure at the nozzle exit.   Because this experiment followed the methods set in a previous coaxial-jet experiment,[14] the test conditions for this experiment were calculated using the same assumptions made in that experiment: steady, isentropic, quasi 1-D flow of a calorically perfect gas at $M=1.8$ and an exit pressure of 1 atmosphere.

CHAPTER 3 - INSTRUMENTATION

3.1 Temperature and Pressure Measurements

All temperatures were measured using T-type thermocouples. Each thermocouple was wired to an Omega-CJ cold junction compensator to provide an ice-point reference. The inherent error in the thermocouple wires was 1 $^\circ$C over the temperature range in this experiment.[17]

All pressure readings within the flowfield and nozzle assembly were measured using strain gauge type pressure transducers from various manufacturers. These pressure transducers varied in range from 0-34.5 kPa (0-5 psia) to 0-1034 kPa (0-150 psid). Each transducer calibration was checked using a pressure balance/pump, and if necessary, recalibrated before the experiment to ensure it was functioning properly ($< 0.5\%$ error in slope from known applied pressures). Three or four pressures were applied to each transducer, namely, atmospheric pressure and several greater pressures, together spanning the operating range of the respective transducer. Pressure transducer signals were processed by the data acquisition system, allowing the calibration slopes and offsets of each transducer to be modified accordingly to produce accurate pressure readings. Previous experience[16] has shown that pressure readings with this particular data acquisition system vary less than 0.3% over the course of an experiment such as this.

3.2 Flowfield Survey

The process of data acquisition and the instrumentation used for this experiment were identical to previous experiments performed in the Mixing Studies Facility. Specifically, the He-O_2 coaxial jet study of Cutler *et al.*[14] is the source from which this experiment obtained its method of data collection.

Four probes were mounted inline on a rake (figure 3), which was itself attached to a translation stage. These probes were a Pitot probe, a stagnation temperature probe, a gas-sampling probe, and a cone-static pressure probe which was not used in this study. The rake was then used to survey the flowfield. Because the model is axisymmetric, only a single sweep across the jet was needed with each probe to record the total pressure, total temperature, or gas composition of the jet for a given axial position.

The translation stage, capable of traversing along the *y*- and *z*-axes, consists of two linear actuators, each driven by a stepper motor. A Compumotor Plus stepper motor and Klinger Model CD4 stepper motor moves the stage in the *z*- and *y*- directions, respectively. Both motors were controlled by a PC that runs the entire data acquisition process. This rake assembly was mounted to the side of the model, and oriented so that rake sweeps were parallel with the exit plane of the flowfield and passed through the axis of the model and jet. A level was used when mounting and securing the translation stage, ensuring that the probe sweeps were in fact parallel to the nozzle-exit plane.
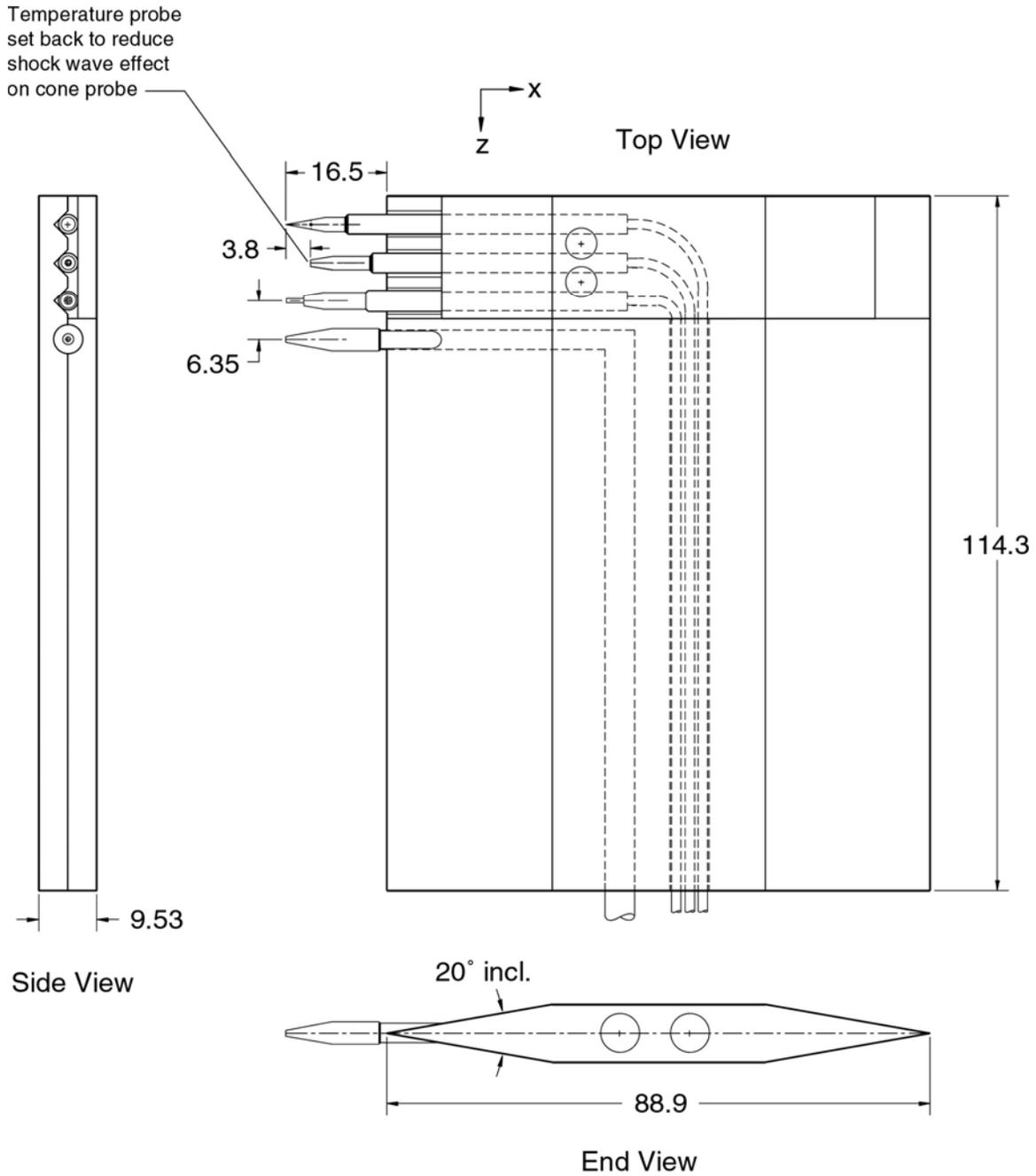
(All dimensions in mm)

Figure 3   Flow field survey probes and rake assembly, from Doehner[16]

The stagnation temperature of the flow was measured using a fast-response thermal probe, Model 300-D050-07-T from the Paul Beckman Company (figure 4a). A miniature thermocouple junction attached to the tip of a 0.20 mm diameter needle is housed inside a radiation shield. Two 0.30 mm holes have been drilled in this shield on

opposite sides of the needle. This probe has been shown to read total temperature about 0.7% low,[18] which is considered acceptable without further calibration.

The Pitot probe uses the tip of a hypodermic needle with a 0.36 mm I.D. and a 0.64 mm O.D. (figure 4b). It was found by Bryer and Pankhurst[18] that this type of probe is relatively insensitive to misalignment (<1% error for 10° misalignment), and it is likely that errors in Pitot pressure measurement due to turbulent flow are less than 1%.[19]

The gas-sampling probe in figure 4c was developed by Johnson.[20] The probe tip is conical and diverges from an I.D. of 0.76 mm to 2.29 mm. A normal shock resides in the diverging portion of the probe, and the flow travels to the gas composition analyzer subsonically. All subsequent tubing I.D. is at least 2.29 mm to ensure the flow remains unchoked.   Johnson[20] has shown that the bow shock is swallowed by the probe tip using Schlieren flow visualization. This probe's sensitivity to misalignment of 15° or less is known to be small.[21]


a) Stagnation Temperature Probe

b) Pitot Pressure Probe

c) Gas Composition Probe
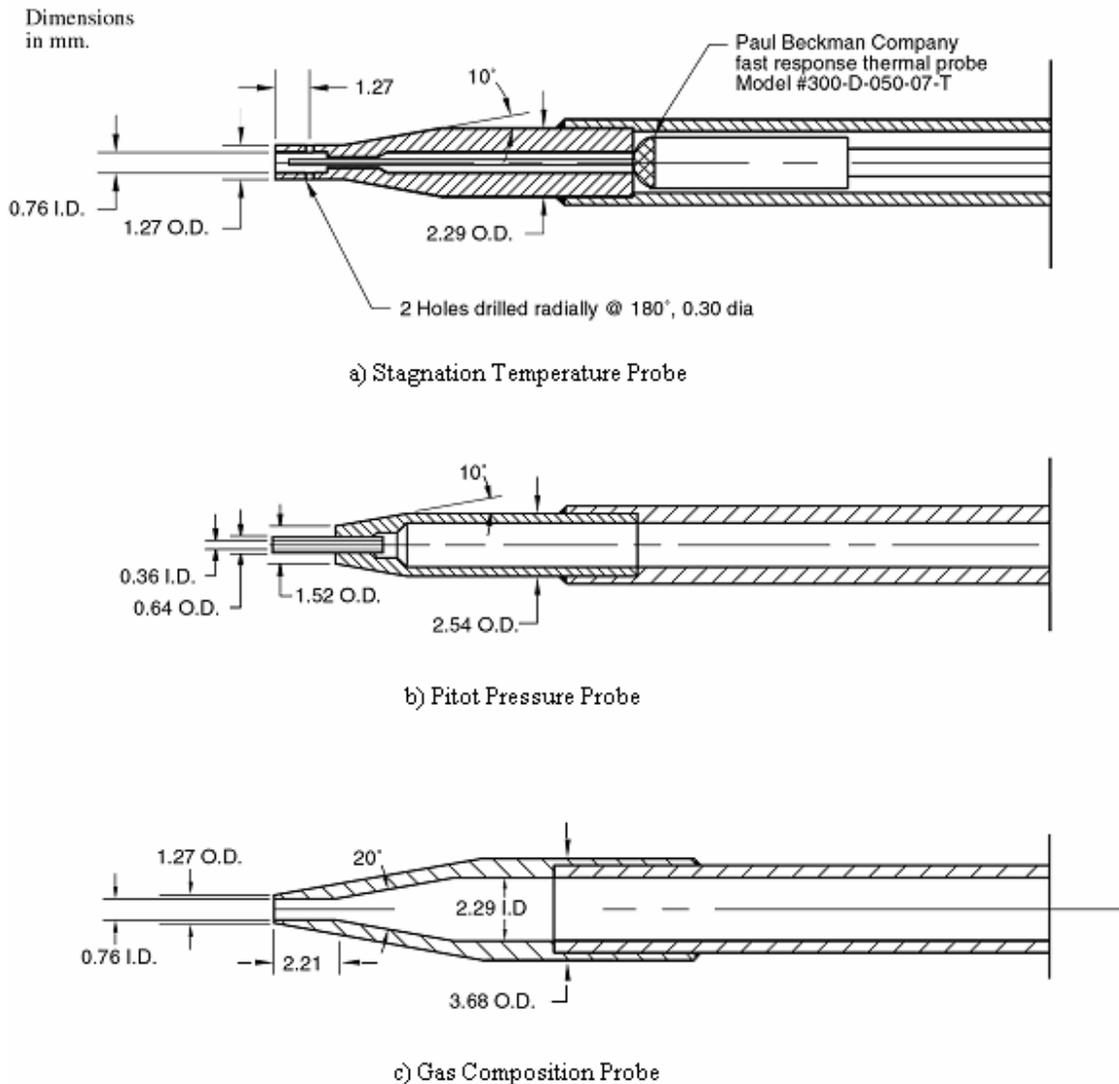
Figure 4   Flow field survey probes, from Doehner[16]

3.3 Gas Composition Analyzer

In order to accurately characterize the mixing, it was necessary to measure the mole fraction of argon in the flowfield. Doerner describes a gas composition analyzing device,[16] modified from a system built by Johnson,[20] using hot film anemometry to determine the composition of a binary gas mixture (figure 5). In short, the gas composition probe diverts a fraction of the flow into the analyzer in which a hot film is fixed. Here, the temperature and pressure of the flow are forced to known values (0 deg C and 1 atmosphere), while the velocity is constrained by a critical flow orifice located downstream of the hot film, allowing the mole fraction of the flow to be determined as a function of a voltage measurement across the hot film.
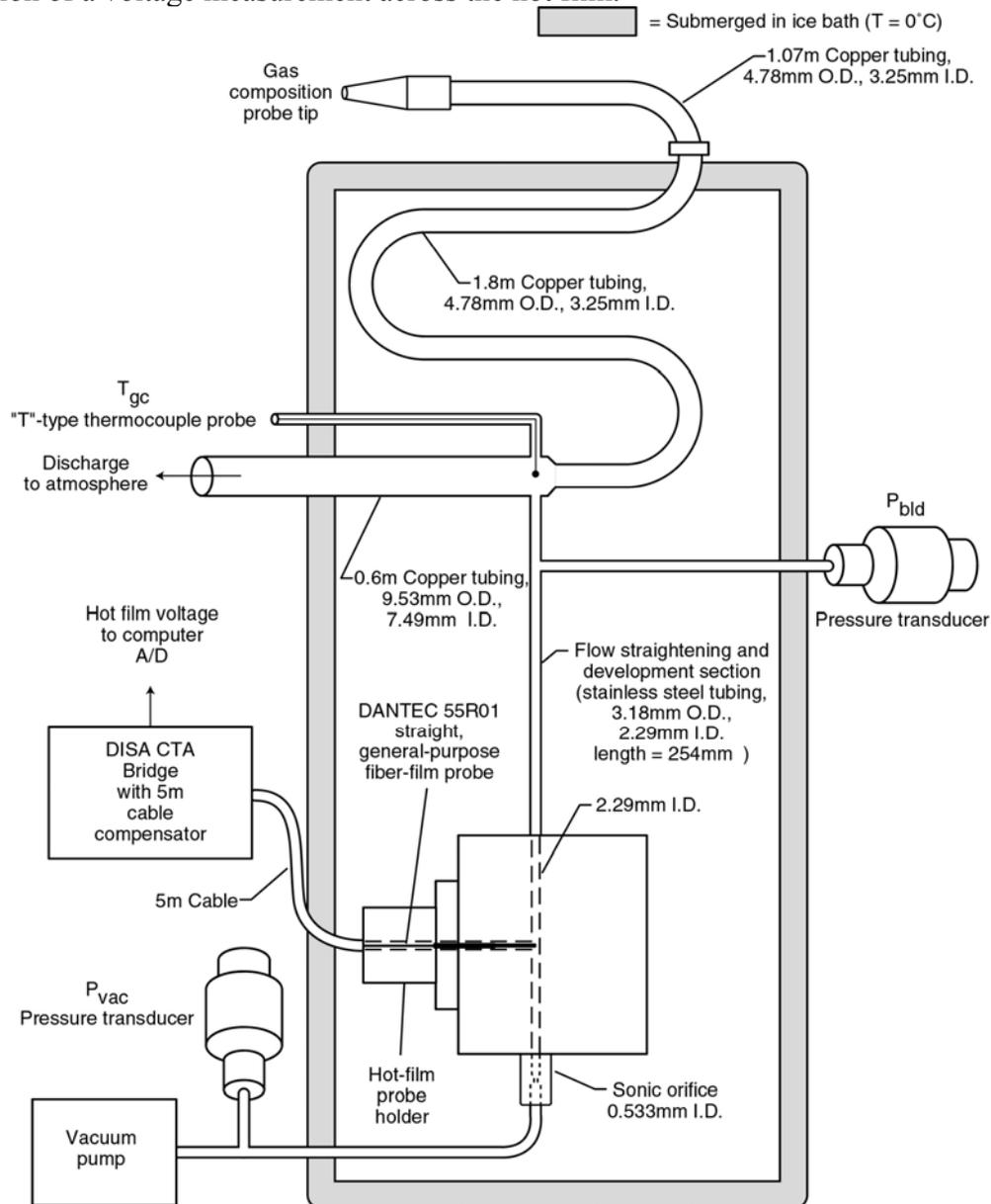
Figure 5   Gas composition analyzer system, from Doehner[16]

The hot film sensor was connected to a DISA Type 55M10 constant temperature anemometer bridge. The overheat ratio, the ratio of hot film operating voltage to hot film voltage at ambient temperature, was set to 1.56.

The gas composition analyzer was calibrated using known mixtures of argon and air. These mixtures were obtained using two Tylan General Digital Mass Flow Controllers (DMFCs), model number DFC 2911V; one connected to a source of pure argon and the other to an air source. A typical calibration curve can be seen in figure 6.

$$y = 2.5998x^4 - 52.554x^3 + 397.76x^2 - 1337x + 1686$$
$$R^2 = 1$$
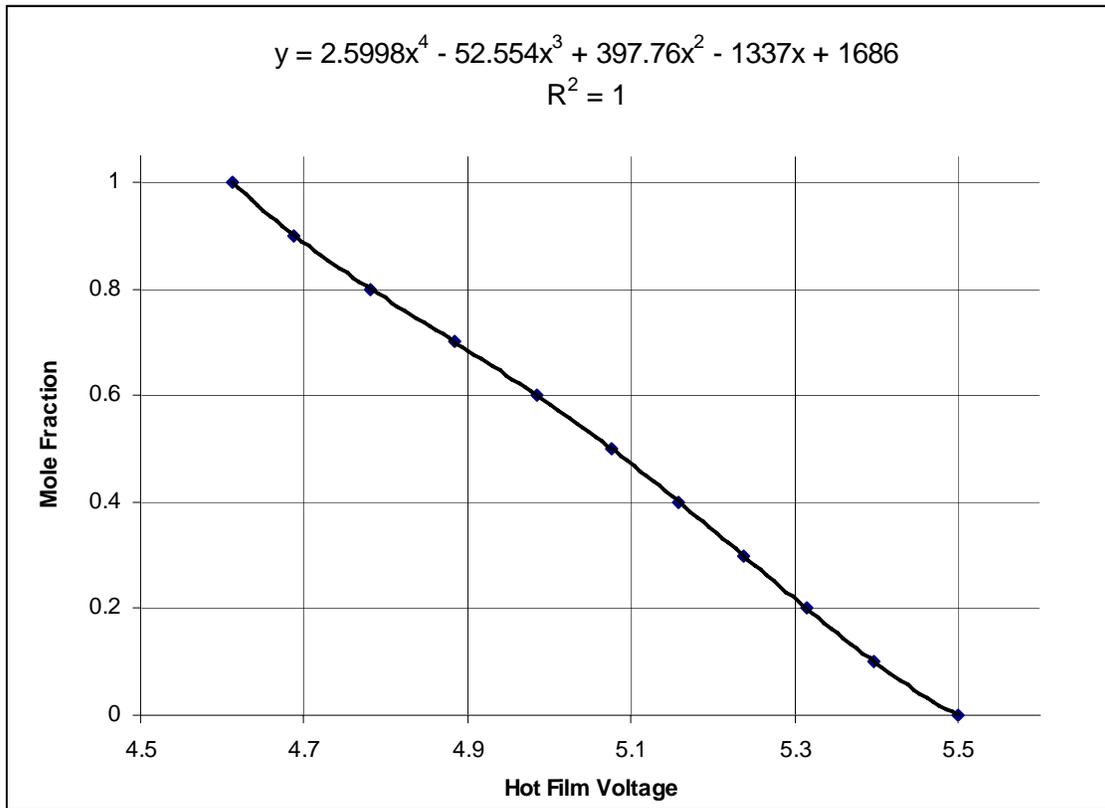
Figure 6   Typical hot film calibration and curve fit

These DFMCs have been used in previous experiments and consequently, one was calibrated for controlling air and the other for a mixture of 95% He/ 5% O_2. A correction factor has been calculated and used to control the flow of argon using the flow controller calibrated for the helium mixture. Using the correction factors listed for argon and a 95% helium mixture with respect to the common manufacturer's calibration test gas of nitrogen, the correction factor for 95%He/5%O_2→Ar is found to be

$$Cf_{95\%He-Ar} = \frac{Cf_{95\%He}}{Cf_{Ar}} = \frac{1.385}{1.415} = .979 \ . \tag{3.1}$$

The correction factor for argon was listed in the manufacturer's flow controller manual and the correction factor for the He-O_2 mixture was obtained from calibration sheets returned with the flow controllers after maintenance service.

The calibrations of the gas analyzer drifted slightly so calibrations were done regularly. Generally, one calibration was done in the morning and one in the afternoon.

The gas analyzer was run with pure argon and then pure air immediately before and after experiment runs to ensure the most recent calibration was providing accurate readings. If the mole fraction readings strayed more than half a percent from the known inflow mole fraction before an experiment run, a new calibration was done. The connections on the analyzer system allow for an easy change between the gas sampling probe and the calibration flow controllers. Despite this setup and procedure, the calibration occasionally strayed more than a half percent during an experiment case-run. The error due to this drift was generally 0.5-0.8%. Including the error in mole fraction from the flow controllers[16] (0.5%), the total uncertainty in gas composition readings is

$$\delta\chi = \sqrt{(0.5\%)^2 + (0.8\%)^2} = 0.94\% \tag{3.2}$$

3.4 Data Acquisition System

Every time this system is run, the probe rake makes a single sweep across the nozzle exit along the y-axis. The National Instruments programming environment, LabView, is used to control the rake assembly. The LabView program is set up to initialize the translation stage, measure zero-flow conditions, and then once the flow is commenced and steady, take data as it directs the rake across the flowfield.

A schematic of the data acquisition system is shown in figure 7. All pressure transducers and thermocouples are routed through their own Neff Model 122 DC Amplifier for signal conditioning. The Neffs are set to a gain of 100 and filter out signals with frequencies above 100 Hz. The Neff outputs are fed into a National Instruments AMUX-T64 multiplexer and a PC employing a NI AT-MIO-16E-10 analog-to-digital converter. The LabView program reads all voltages, rescales the signals by 1/100, implements the calibrations, and records the data to disk. At every probe position, the program pauses to allow for probe response. The response times for the probes used in this experiment have been calculated and discussed in Doehner[16] in which a pause time of 0.3 seconds was determined to be sufficient. After this brief pause, the program reads all channels 500 times at 2500Hz and averages the readings before commanding the translation stage to move by a preset increment to the next point.
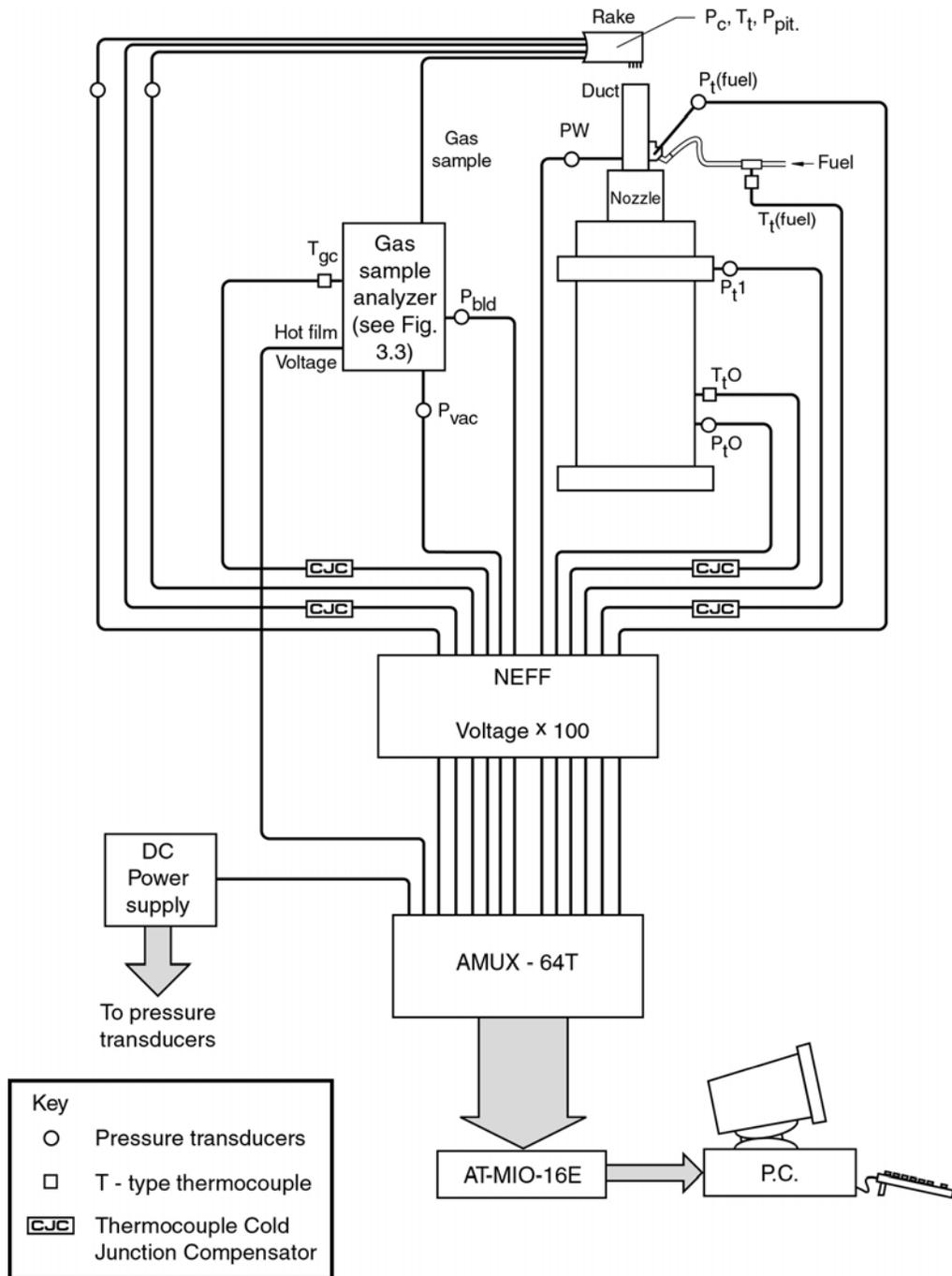
Figure 7   Data acquisition system, from Doehner[16]

3.5 Operating Procedure

Data were collected at 17 planes of varying axial (x) distance from the center nozzle-exit plane (Table 1), the first 14 of these planes are those from the previously mentioned He-O_2 experiment while the rest are further downstream (the mixing rate for the present argon case was slower). Gas composition and Pitot pressure were measured at each plane with the exception of Plane 1, where only Pitot pressure was measured.

Total temperature was measured less frequently (Planes 9 and 14) as variations in total temperature were small. Survey measurements were started closest to the nozzle exit and taken in the order shown in Table 1. During a survey, once the test gases reached the required pressure and remained steady, only one probe was used for measurement along the *y*-axis. The gas flow was then turned off, and the next probe was aligned with the *y*-axis and a new survey taken. When all surveys for a plane were finished, the translation stage was raised until the probe rake reached the next streamwise station, and the probes appropriately positioned for subsequent surveys.

Plane	X (mm)	X (in)	Survey(s) taken
1	0.127	0.005	Ppit
2	3.10	0.122	Ppit, MF
3	9.97	0.392	Ppit, MF
4	17.91	0.705	Ppit, MF
5	28.26	1.113	Ppit, MF
6	43.47	1.712	Ppit, MF
7	61.90	2.437	Ppit, MF
8	81.61	3.213	Ppit, MF
9	100.53	3.958	Ppit, MF, Ttot
10	122.12	4.808	Ppit, MF
11	150.85	5.939	Ppit, MF
12	181.61	7.150	Ppit, MF
13	219.51	8.642	Ppit, MF
14	261.20	10.284	Ppit, MF, Ttot
15	325.78	12.826	Ppit, MF
16	386.46	15.215	Ppit, MF
17	452.75	17.825	Ppit, MF

Ppit = Pitot pressure
MF = Mole Fraction
Ttot = Total Temperature

Table 1   Survey planes

A set of stacking stainless steel cylinders was machined specifically to provide a reliable guide for raising the probe rake to the desired locations. A combination of cylinders was stacked on the nozzle exit and the probes were raised to and then secured so the probe tips were even with the stack's top. Once in place, the exact axial distance to the probe tips was measured using feeler gauges, or in the latter planes, a digital caliper. These stacking cylinders are pinned together via center holes which provided an accurate guide for aligning the probes with the center of the coaxial jet.

3.6 Measurement Uncertainty

The measurements and associated uncertainties of various quantities acquired during the data collection process are summarized in Table 2. These uncertainties are represented by error bars in various plots presented in Chapter 5.

	Parameter	Symbol	Value
	Upstream Coflow Pressure	$p_{\text{ref,coflow}}$ (kPa)	581 ± 4.4
	Upstream Coflow Temperature	$T_{\text{ref,coflow}}$ (K)	295.6 ± 3.5
	Upstream Center Jet Pressure	$p_{\text{ref,CJ}} / p_{\text{ref,coflow}}$	1.056 ± .095
	Upstream Center Jet Temperature	$T_{\text{ref,CJ}} / T_{\text{ref,coflow}}$	1.01 ±.012
	Ambient Pressure	$p_{\text{amb}} / p_{\text{ref,coflow}}$	0.175 ± .0011
	Ambient Temperature	$T_{\text{amb}} / T_{\text{ref,coflow}}$	0.992 ± .012
	Nozzle Exit Pressure	$p_{\text{exit}} / p_{\text{ref,coflow}}$	0.162 ± .0025
Rake Probes			varies
	Gas Composition	MF	± .94%
	Total Temperature Probe	T_{t} (K)	-0.70%
	Pitot Pressure Probe	p_{pit} (kPa)	< ± 1.0%

Table 2   Experimental flow parameters

CHAPTER 4 - CFD

The flow in the coaxial nozzle and downstream field has been simulated using the CFD code Vulcan, a structured, finite-volume code that solves Favre-averaged Navier-Stokes equations.[1] The k-omega turbulence model[22] is typically used for computing hypersonic flows within Vulcan at the Hypersonic Airbreathing Propulsion Branch in Langley Research Center (where this experiment took place), and was also used in a similar coaxial-jet experiment.[14] For the sake of consistency, the k-omega turbulence model has been implemented here for each calculation, and in general, the CFD grid and boundary conditions were chosen to allow for easier comparison between this experiment and that of Cutler *et al.*[14]

A structured grid of 188,080 cells is distributed among five blocks and was originally generated for the He-O_2 experiment of Cutler *et al*[14] using a commercial code, Gridgen. Figure 8 shows the grid used, and a closer view of the grid at the nozzle exit can be seen in figure 9 in which only every eighth grid line is shown and the axes are rescaled to spread out grid lines. The boxed in portion has been expanded and is overlaid.
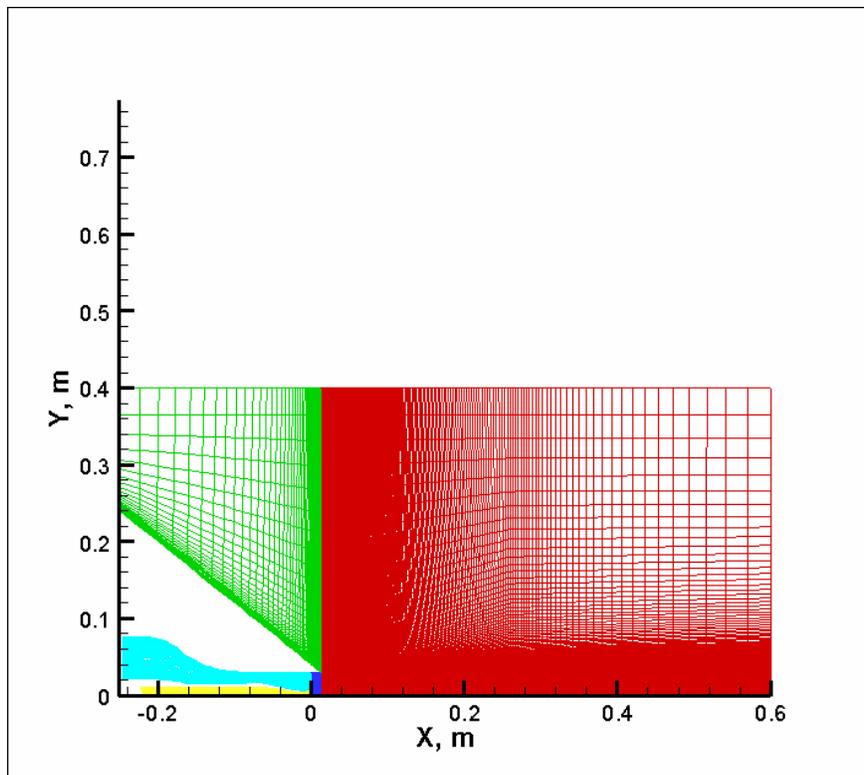
Figure 8   Coaxial jet and flowfield Grid
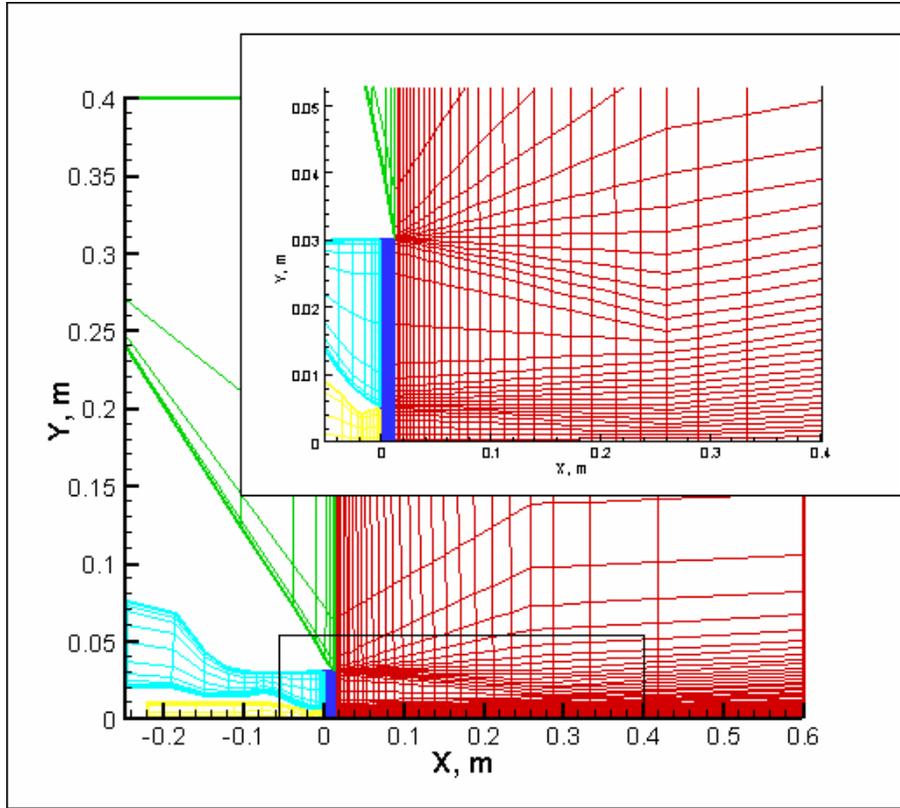
Figure 9   Coaxial jet and flowfield grid, zoom and rescaled

The walls are specified as adiabatic and no slip. The flow is assumed to be axisymmetric. The composition at the exterior boundary is assumed to be air with a density of 1.194 kg/m^3 and pressure of 101.4 kPa. The coflow nozzle inflow boundary condition is air with a total density of 6.85 kg/m^3 and a total pressure of 581 kPa, based on measured temperature and pressure in the coflow plenum. The inflow boundary condition of the center jet nozzle is argon with a total density of 10.11 kg/m^3 and total pressure of 628.2 kPa and was calculated using an upstream static pressure measurement as well as the ratio between the sonic throat area and the area at which the upstream static pressure was measured, assuming quasi one-dimensional flow.

Because the grid points are clustered near nozzle exits and walls (to help resolve boundary layers, and shocks from nozzle lips), the grid cells increase in size along the *x*-axis as seen in figure 9 where the grid point distribution is easier to observe. To maintain confidence in comparisons between CFD results and experimental data, discussion will be confined to the region upstream of and including Plane 14 (*x* = 261 mm), downstream of which the grid spacing becomes too large.

There have been modifications made to the Vulcan code in the time between the He-O$_2$[14] experiment and this experiment. A computation has been run using the He-O$_2$ mixture as the center-jet gas to make sure that the code is still performing as before and that changes made in the code do not affect the solution. Pr_t and Sc_t were both given values of 0.75 and the He-O$_2$ calculation ran for 35,000 iterations on the fine grid. The normalized Pitot pressure from this He-O$_2$ case is plotted in figure 10 with the experimental data at plane 14 (*x* = 261 mm, the most downstream plane). When

compared with the same plane in the CFD comparison from the initial He-O$_2$ experiment in figure 11, it is apparent that the results are consistent; the mixing in the center He-O$_2$ jet is well predicted while the coflow mixing is noticeably underpredicted using both versions of Vulcan. Therefore, it is reasonable to assume that the recent changes in the code will have no effect on any calculated predictions of the jet flow.
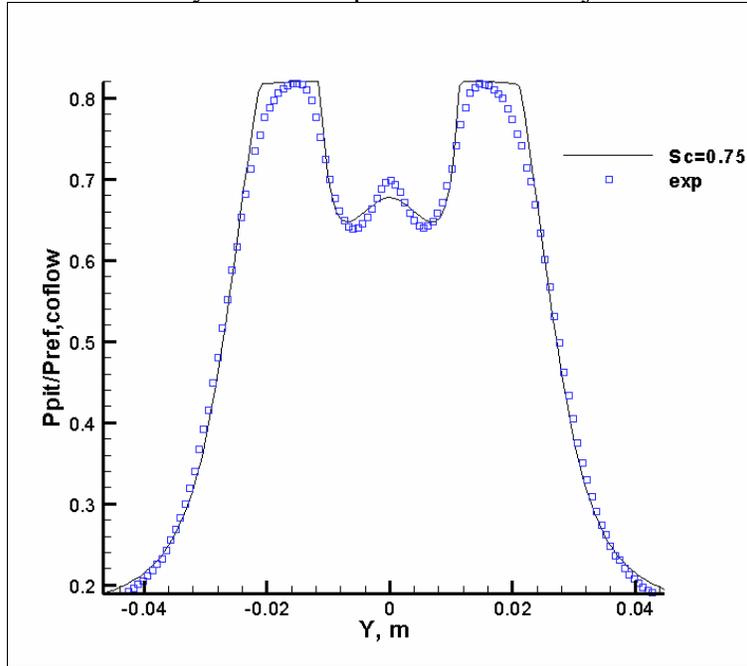

Figure 10   Comparison of recent CFD and He-O$_2$ P$_{pit}$ data at Plane 14
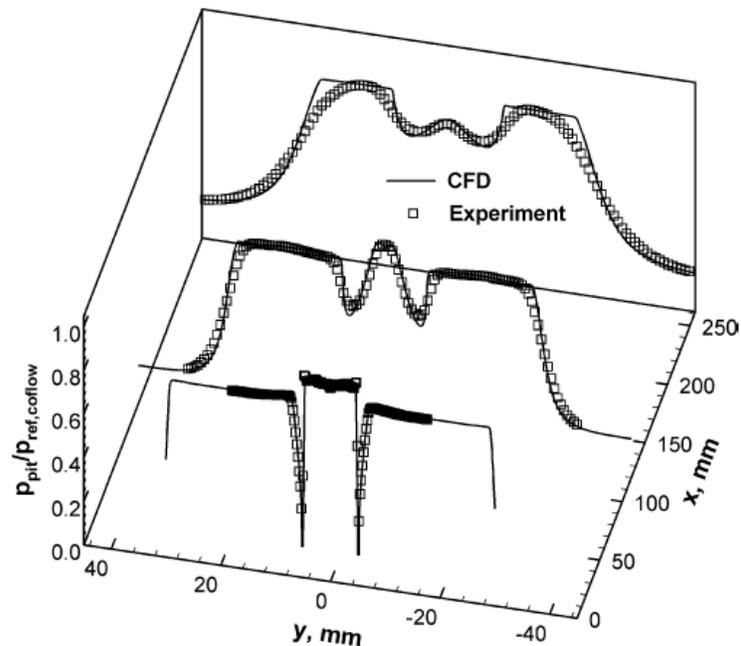
Figure 11   Comparison of old CFD vs. He-O$_2$ P$_{pit}$ data, from Cutler _et al._[14]

CFD calculations have been done with and without the Pope correction[22] for the round jet-plane jet anomaly. The turbulent Prandtl number and turbulent Schmidt number were assumed constant within a given calculation, and several calculations were

performed with values of Sc_t as 0.1, 0.25, 0.5, and 0.9 while keeping $Pr_t = 0.9$. A case was also run with Sc_t and Pr_t both equal to 0.5. The Courant-Friedrichs-Lewy number regulates the time step within a given CFD calculation, and for each calculation it was ramped from 0.1 to 3.0 during a few thousand iterations at each grid level. Convergence was slow on the fine grid; typically, the calculations were run with 45,000 iterations on the fine grid and the L2 norm was reduced by more than 4.5 orders of magnitude.

The CFD solutions require more time for convergence in regions further downstream and closer to the axis of symmetry. To ensure that the solutions were in fact converged, the CFD calculation in which Sc_t is 0.5 (which will later be shown to be the most accurate case) was run for 35,000 more iterations. Figure 12 shows the combined residual history of the initial 45,000 iterations as well as the final 35,000 iterations of this CFD case. This figure plots the normalized L2 residual (Rel_{L2}) defined by the Vulcan CFD manual.[23] This solution was obtained by starting the calculation from a restart file of a different CFD case, and a dividing line has been inserted in figure 12 to separate the two calculations and show where the case in which $Sc_t = 0.5$ begins 45,000 iterations on the fine grid. This plot shows that the solution has not completely settled after 45,000 iterations, but it can be seen that the residual history has leveled off after 80,000 iterations.
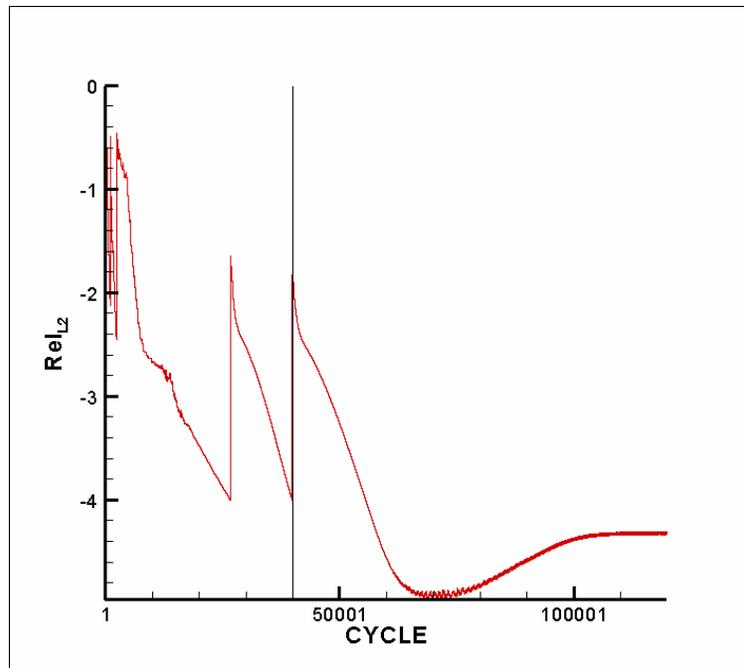
Figure 12   Residual history where $Sc_t = 0.5$

Figure 13, in which the Pitot pressure has been divided by the total plenum pressure, shows that there is no discernible difference between the Pitot pressures obtained with 45,000 and 80,000 iterations at Plane 14 ($x = 261$ mm). Due to the nature of the code, M on the center line converges more slowly than most variables. Figure 14 shows very little change in centerline M over the course of the last 35,000 iterations. With the evidence presented in figures 13 and 14, it can be assumed that the solution has converged satisfactorily after 45,000 iterations.
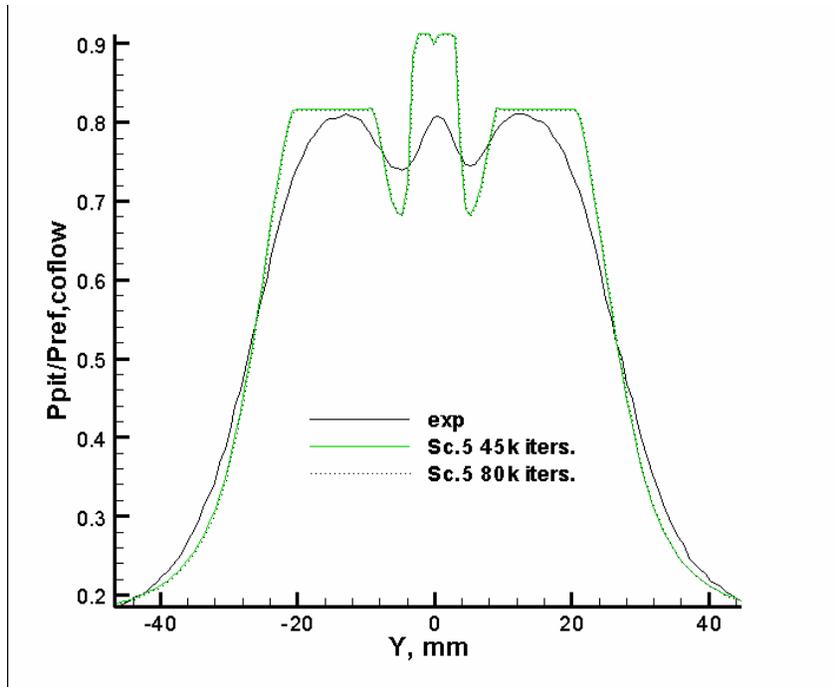
Figure 13   Comparison of Pitot pressures separated by 35,000 iterations
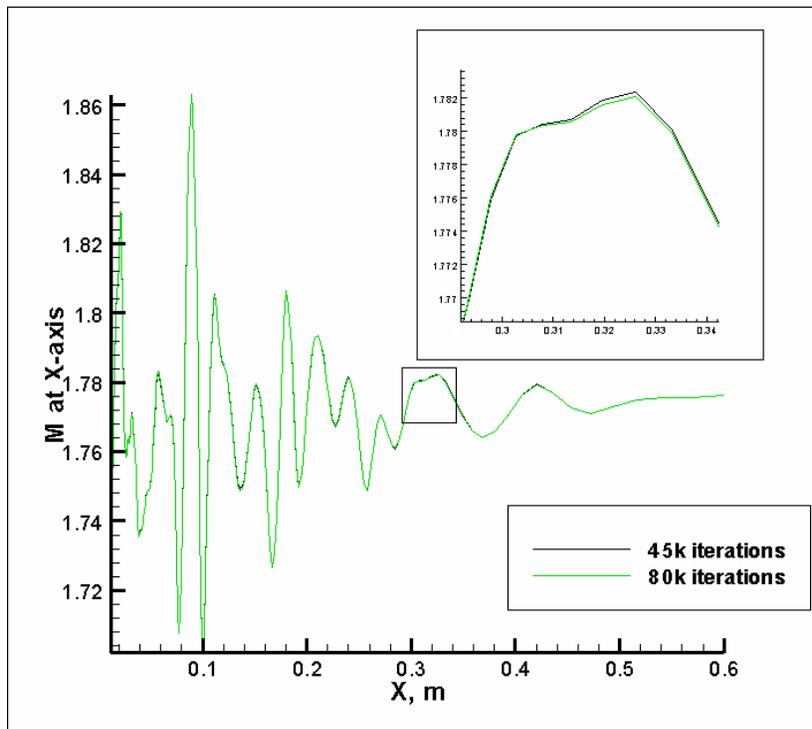

Figure 14   Comparison of centerline Mach number

A closer examination of the CFD solution for the low speed entrainment is presented in figures 15 and 16. Velocity streamlines have been included in a contour plot of the x-direction velocity, u, for both the argon and He-O_2 cases, respectively. The flow is smooth and steady and the right (downstream) boundary of the grid is an exit plane for

the flow. Although the path of entrainment is not quite what was expected, it is of such relatively low speed, and is smooth and steady, so that the jet mixing calculation is not adversely affected.
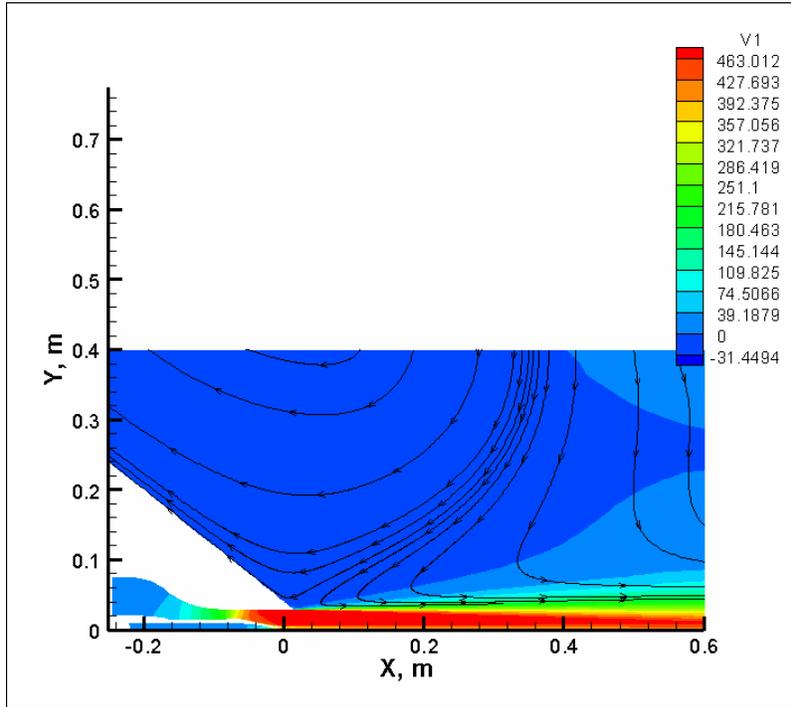
Figure 15   Streamlines of CFD calculation of argon coaxial jet
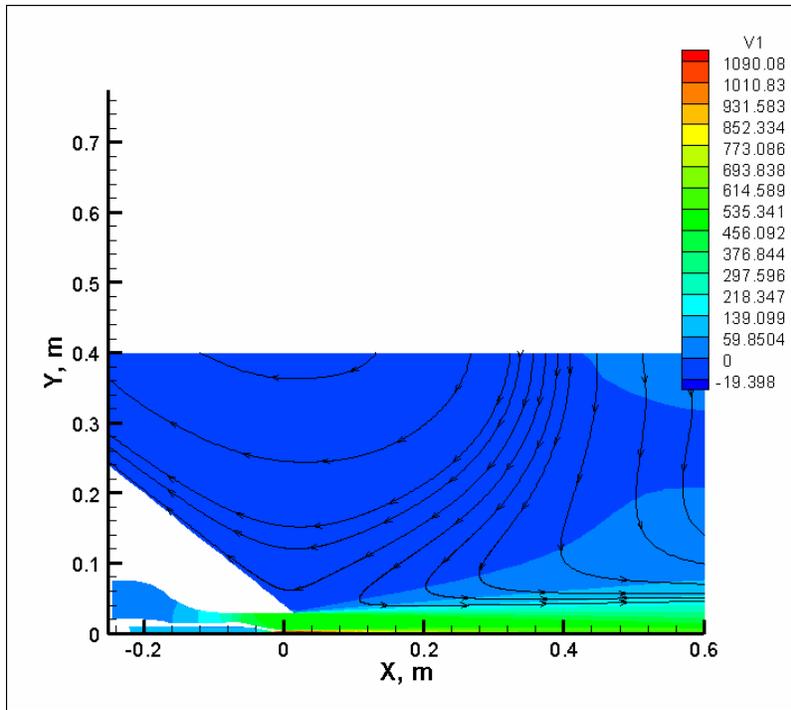
Figure 16   Streamlines of CFD calculation of He-O$_2$ coaxial jet

The solution convergence was checked as previously discussed in this chapter; however grid convergence was not checked. In the comparisons of CFD predictions and experimental measurements presented in the following chapter, it is apparent that the computations underpredict the mixing of the coaxial jet. If the grid was under-resolved, the result would be too much mixing or diffusion, not too little, as seen in Chapter 5.

CHAPTER 5 - RESULTS

5.1 Probe Data

This chapter presents the flowfield data acquired in this experiment as well as comparisons of this data to computational predictions of the coaxial jet made using a CFD code developed by NASA, Vulcan.[23] In particular, it is hoped that these comparisons illuminate the ability of the turbulence model to accurately predict the development of the coaxial jet.

Probe surveys were taken along the y-axis at planes of varying axial (x) distance from the center-jet nozzle exit, as indicated in Table 1. As previously discussed, these surveys consist of mole fraction and Pitot pressure measurements, as well as total temperature measurements at Planes 9 and 14.

The experimental data for the argon coaxial jet are shown in figures 17 - 18 side-by-side with the data from a previous experiment[14] in which a He-O$_2$ mixture was used as the center-jet gas. Figures 17a and 17b show the Pitot pressure survey readings normalized by the plenum/reference pressure (upstream total pressure) at each plane from the argon and He-O$_2$ experiments, respectively. The unvarying total pressures in the center and coflow jets are reflected by the regions of constant Pitot pressure in these plots. The slight deviations visible are the result of weak shocks propagating from the nozzle-exit walls. The region of mixing between the jets of argon and air is marked by a Pitot pressure deficit, due in part to the downstream convection of low total pressure flow in the nozzle boundary layers. The downstream broadening of this pressure deficit represents the growing mixing layer between the two jets.

In figures 17a and 17b, a slight total pressure deficit can be seen at the center of the flow. This has been noted and explained by Cutler *et al.*,[14] and is the result of a weak normal shock formed at the x-axis where inward-propagating expansion waves intersect. This trough can be seen in the argon jet as far as 122 mm downstream of the nozzle exit, where it becomes obscured by the mixing layer between the center jet and coflow. However, in the He-O$_2$ case, the deficit is only visible until x =101mm, indicating quicker mixing of the coflow into the center jet.
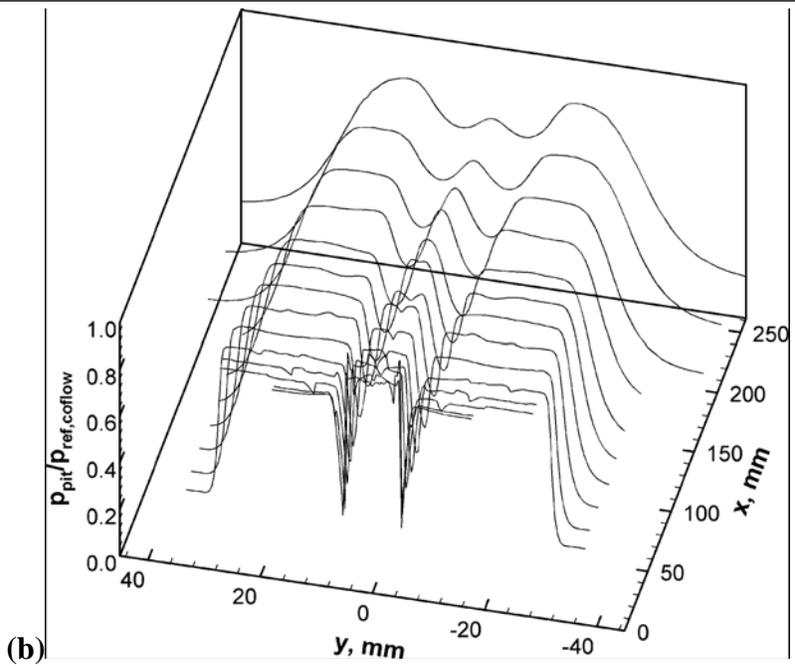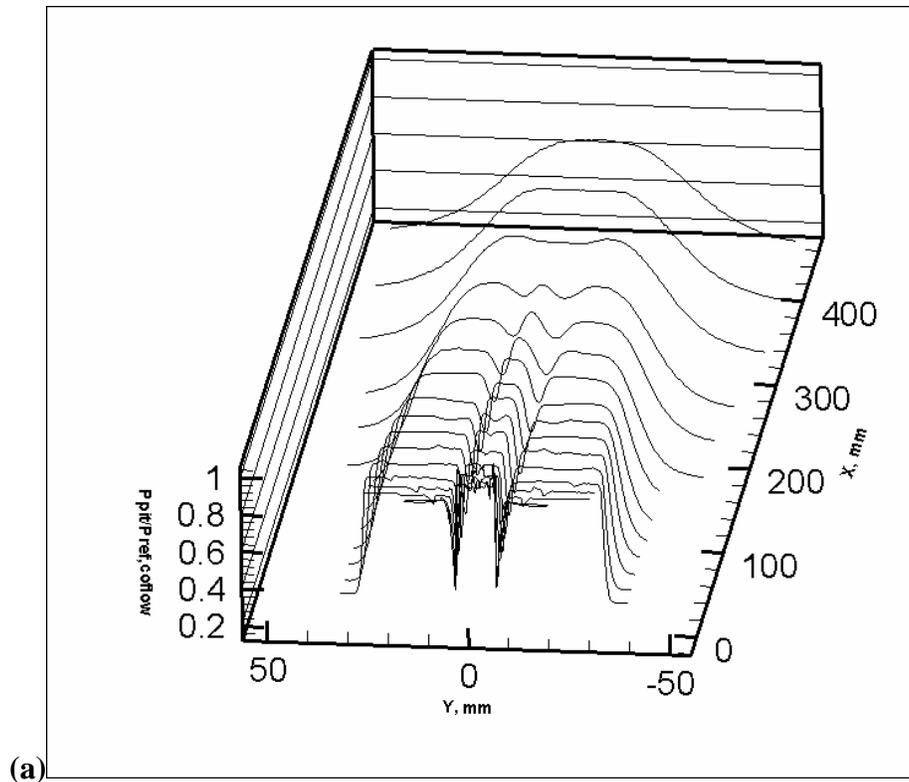
**Figure 17(a)Argon case Pitot pressure measurements. (b) He-O₂ case Pitot pressure measurements, from Cutler *et al*.[14]**

(a)

(b)
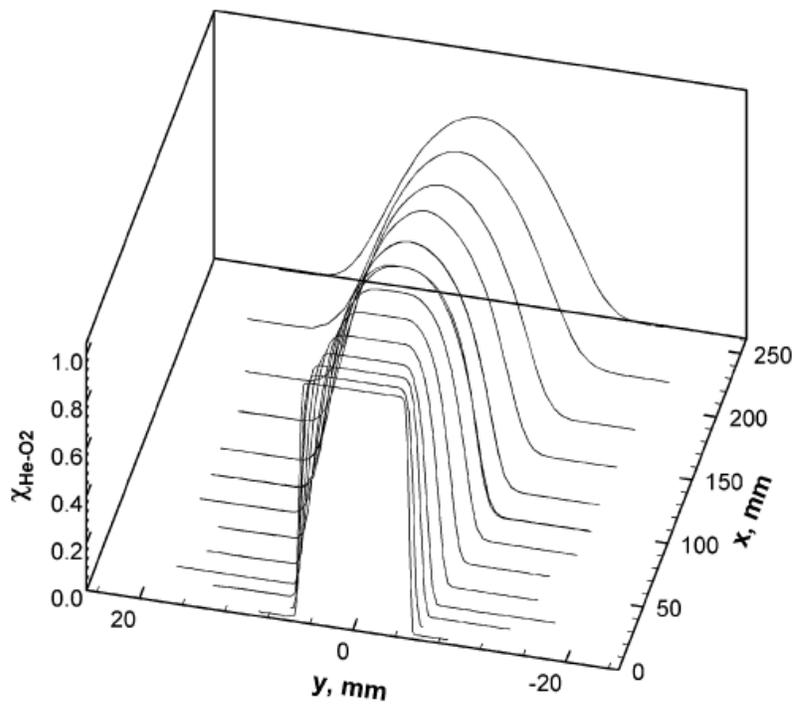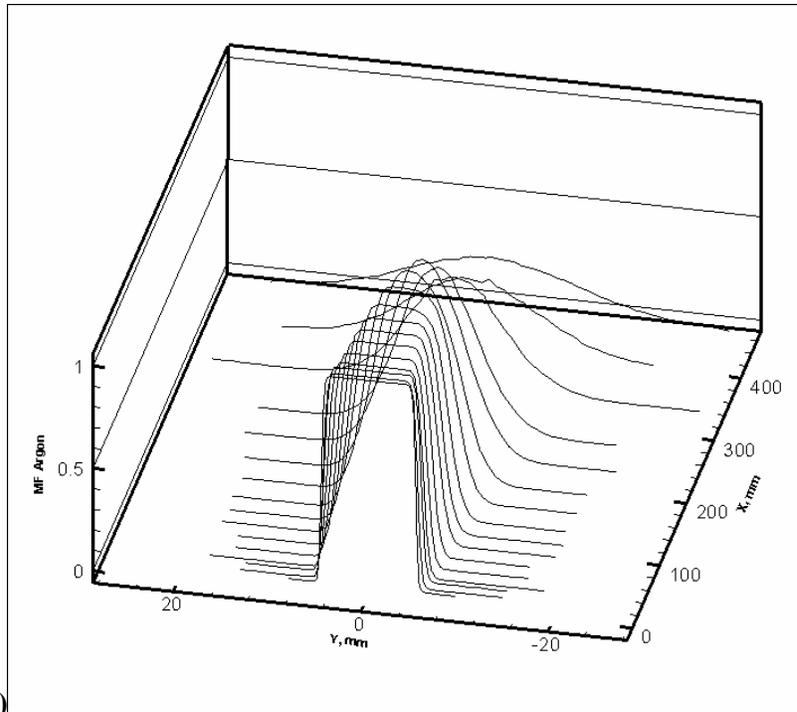
Figure 18(a)Argon mole fraction measurements. (b) He-O$_2$ mole fraction measurements, from Cutler *et al.*[14]

Figures 18a and 18b show the mole fraction as a function of radial location (*y*) at each plane from the argon and He-O$_2$ experiments, respectively. The mixing between the

coflow and center jet is reflected in the smoothing and eventual flattening of the plots with increasing distance from the nozzle exit. Further examination reveals that this freestream mixing rate is faster in the He-O_2 experiment. The last plane at which $\chi = 1$ anywhere within the center jet is Plane 10 ($x = 122$mm) in figure 18b and Plane 12 ($x = 182$mm) in figure 18a, again signifying that the mixing between the argon and coflow is slower than that of the He-O_2 mixture (no mole fraction surveys taken for Plane 1, $x = 0.127$ mm). The additional three survey planes visible in figure 18a were added to the argon data set to ensure that the degree of jet mixing reaches or surpasses that in the He-O_2 experiment.[14]

5.2 Comparisons with CFD

The following figures present a comparison of experimental results with CFD calculations. Figure 19 shows the experimental and calculated plots of the Pitot-to-plenum pressure ratio, $P_{pit}/P_{ref,coflow}$, at the nozzle exit (Plane 1, $x = 0.127$ mm). The various calculations produce nearly indistinguishable results from each other and agree well with the experiment. This indicates that the code is predicting the flow within the nozzle correctly, and suggests that any downstream divergence of the computation from the experiment is caused by deficiencies in the jet modeling.
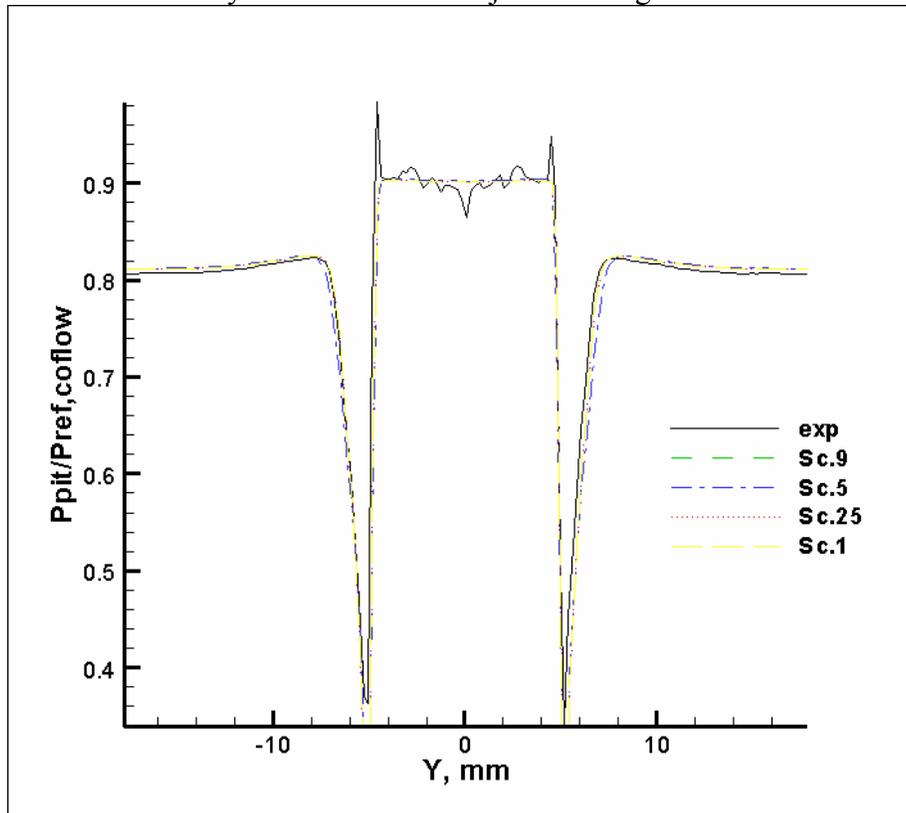

Figure 19   Pitot pressure Plane 1

Moving downstream, the Pitot pressure normalized by plenum pressure is plotted in figure 20 for the experimental results and CFD predictions at Plane 9 ($x = 101$ mm). All CFD cases appear nearly identical and track the experiment well. The coflow total

pressure is well predicted here as is the previously mentioned pressure deficit in the center jet. Figure 21 shows experimental and calculated plots of mole fraction with respect to radial location at Plane 9 ($x = 101$ mm). Values for Sc_t of 0.25 and particularly 0.1 result in poor solutions, whereas values of 0.5 and 0.9 produce accurate ones. In both Figures 20 and 21, error bars have been included to reflect the experimental measurement uncertainty within these plots.
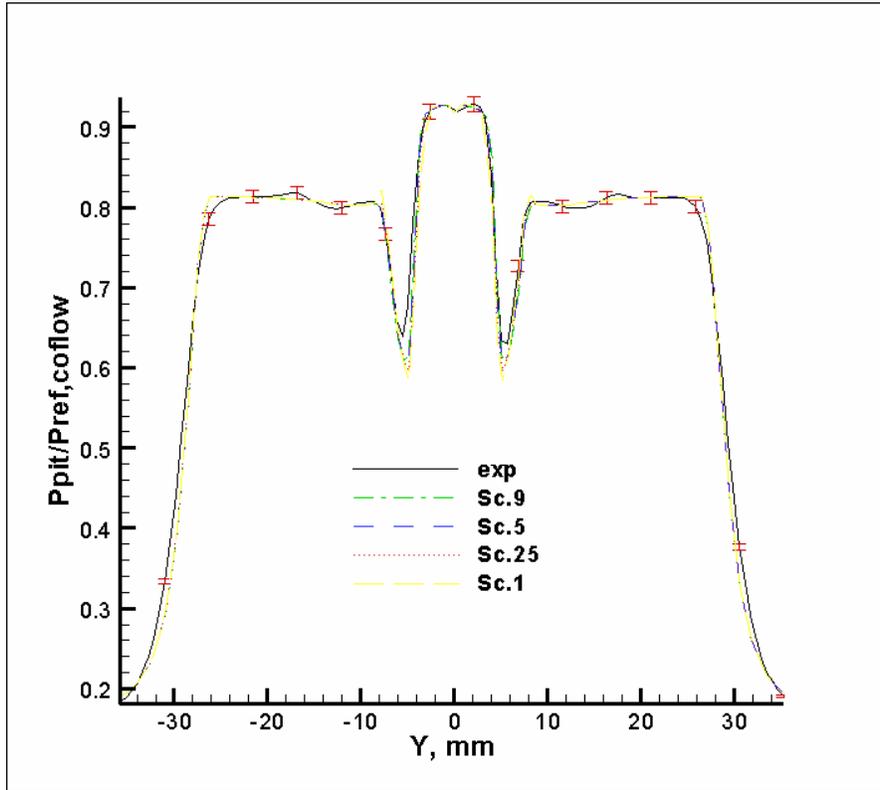

Figure 20   Pitot pressure Plane 9
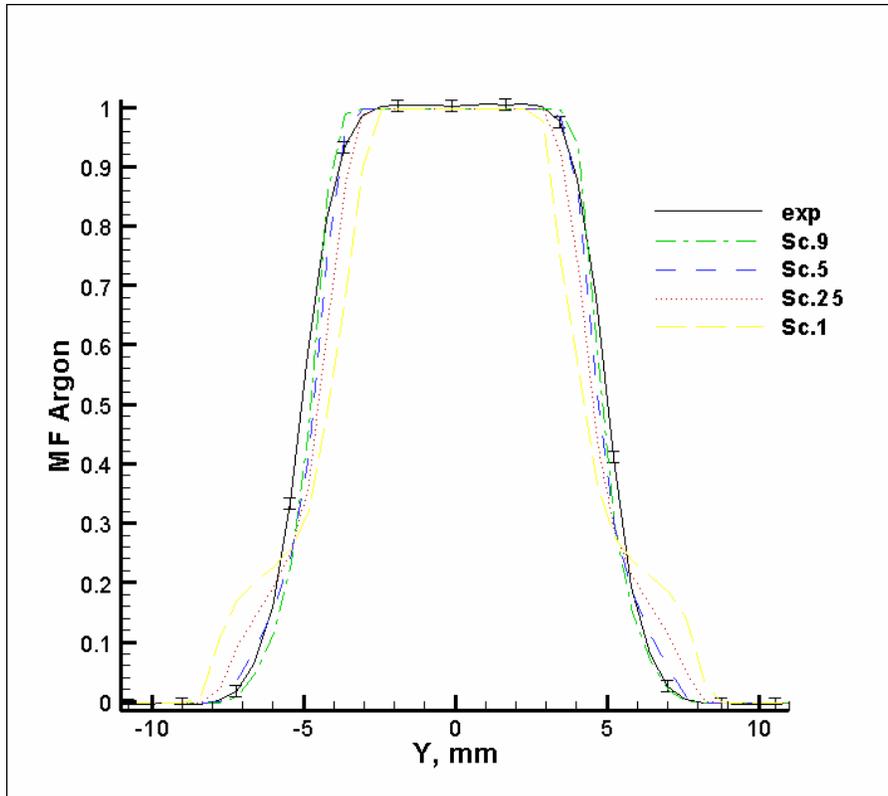
Figure 21   Mole fraction Plane 9

The Pitot-plenum pressure ratio at Plane 14 ($x = 261$ mm) is plotted in figure 22. Again, the CFD solutions are very close to one another, but here they do not represent the experiment well. The measured extent of mixing is underpredicted, reflected in figure 22 by the greater freestream pressures and mixing-layer pressure deficit, as well as the pressure deficit in the center jet, indicating that the coflow has not yet mixed into the center of the argon jet. Figure 23 compares the species mixing at Plane 14 ($x = 261$ mm), and it is apparent that all CFD cases greatly underpredict the mixing in the flow. Also, as previously noted in discussion of figure 22, the calculations predict that a region of pure argon still exists represented in figure 23 where $\chi = 1$.
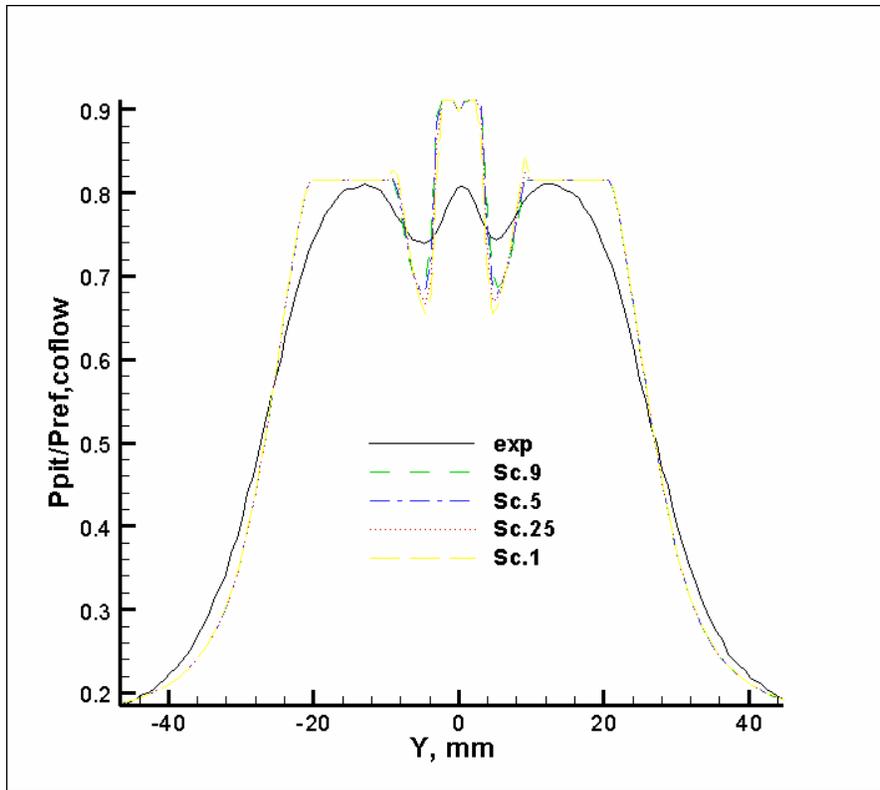
**Figure 22   Pitot pressure Plane 14**
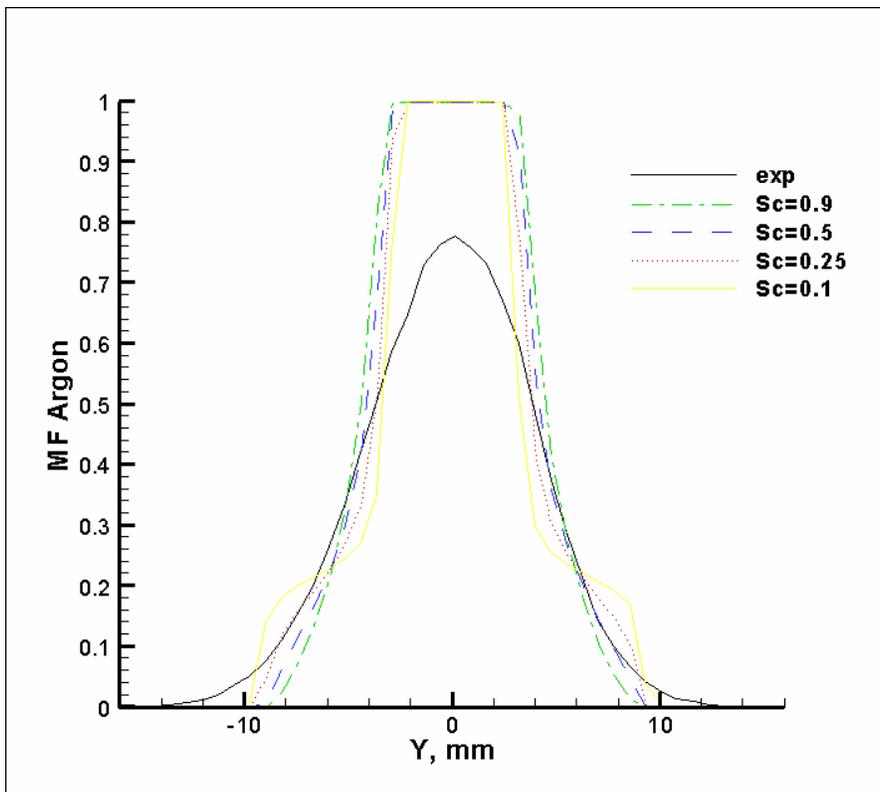
Figure 23   Mole fraction Plane 14

The measured and predicted total temperatures normalized by the coflow-plenum total temperature are plotted in figure 24. Within the coflow freestream, the experimental data are about 1% less than the calculated temperature of the coflow as shown by the larger flat region in the plot. This is not uncommon for this type of probe, and the error bars included reveal that this is an acceptable deviation. However, any similarity ends here, as the overall agreement between the predicted and measured total temperature is poor. In particular, there is more than 5% difference in the calculated and experiment center jet total temperature. Because the argon bottle supply is located outside, the supply temperature fluctuates with outdoor conditions. The calculations done were based on an average supply gas temperature, so the data were reviewed to see if this average was significantly different from the temperature at which the total temperature data were taken, but the data did not show more than a 1% difference from the average temperature. In figure 24, it appears that the discrepancy between the computational and experimental total temperatures is a result of a boundary condition problem. According to the plot, either the argon bottle temperatures were colder than thought, or heat loss occurred prior to the nozzle exit plane. It is uncertain as to how either may have happened to this degree.
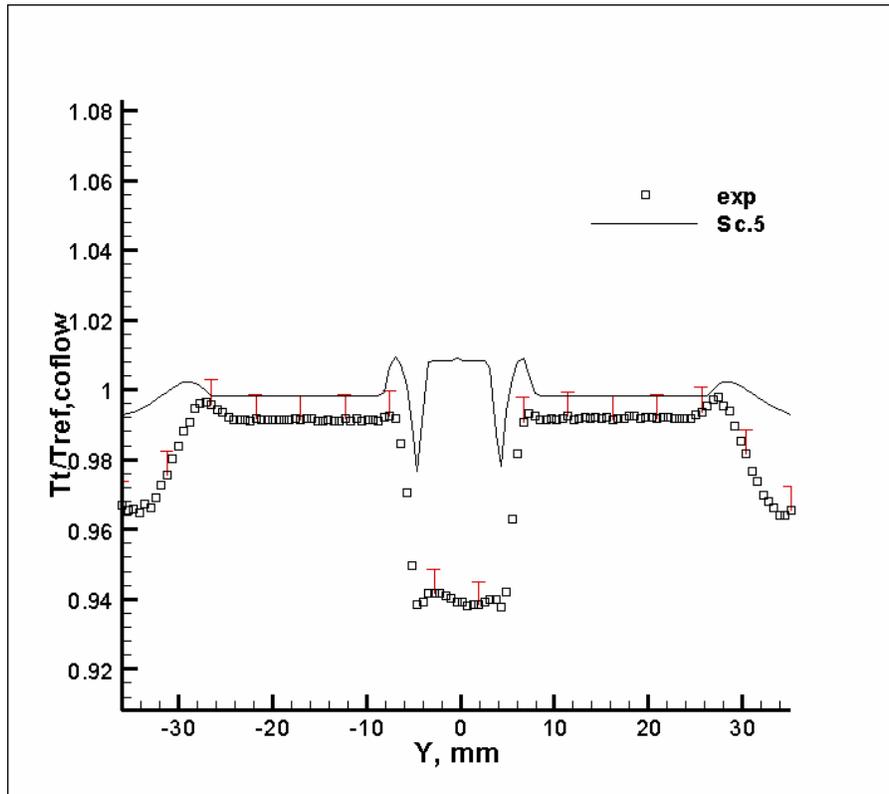

Figure 24   Total temperature Plane 9

As previously mentioned, CFD calculations were done using the Pope correction. However, because the Pope correction tends to decrease the mixing rate, it does not offer a more accurate solution as figures 25 and 26 show. Figure 25 compares calculations, with and without the Pope correction, of mole fraction at Plane 11 ($x = 151$ mm) with $Sc_t = 0.5$. Figure 26 displays normalized Pitot pressures from the same calculations. These

plots confirm that the CFD code better predicts the flowfield without implementing the Pope correction.
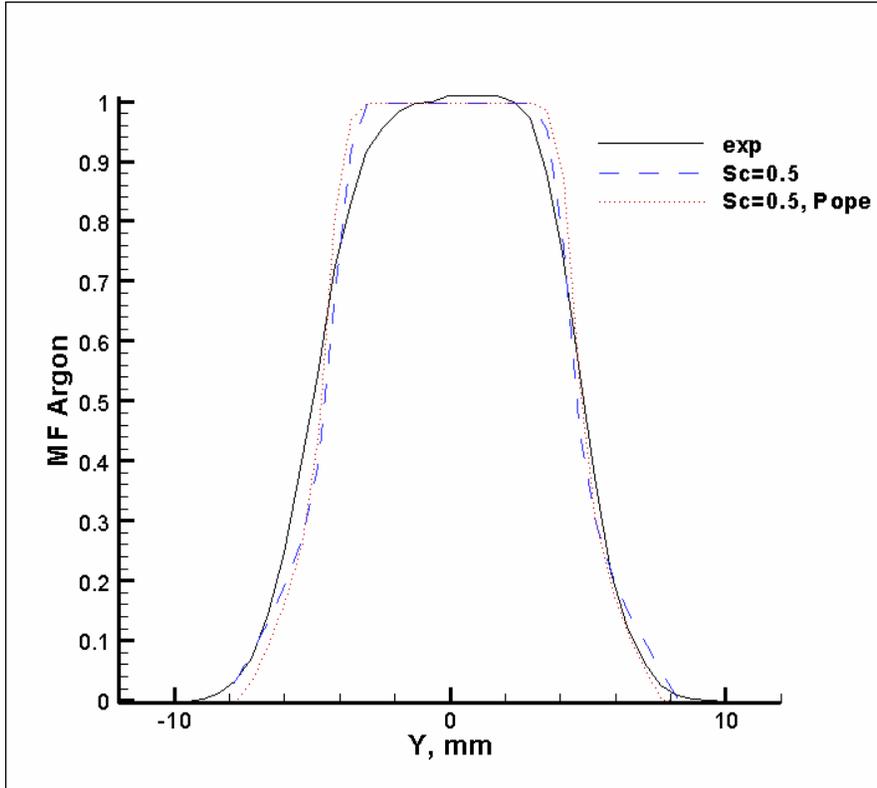
**Figure 25   Mole fraction w/ Pope correction Plane 11**
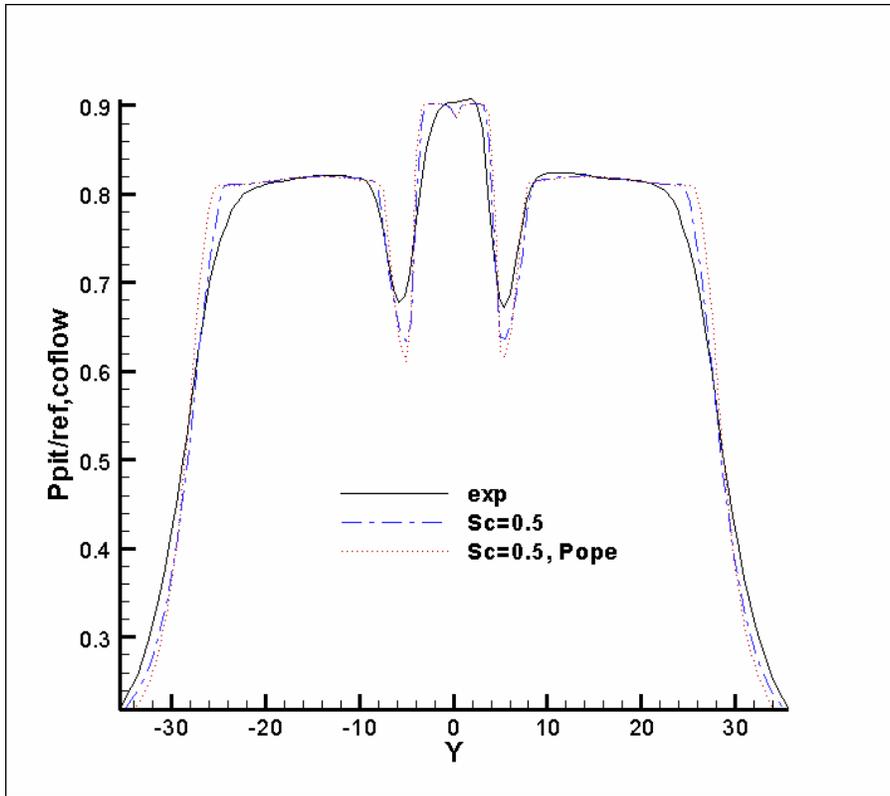
**Figure 26   Pitot pressure w/ Pope correction Plane 11**
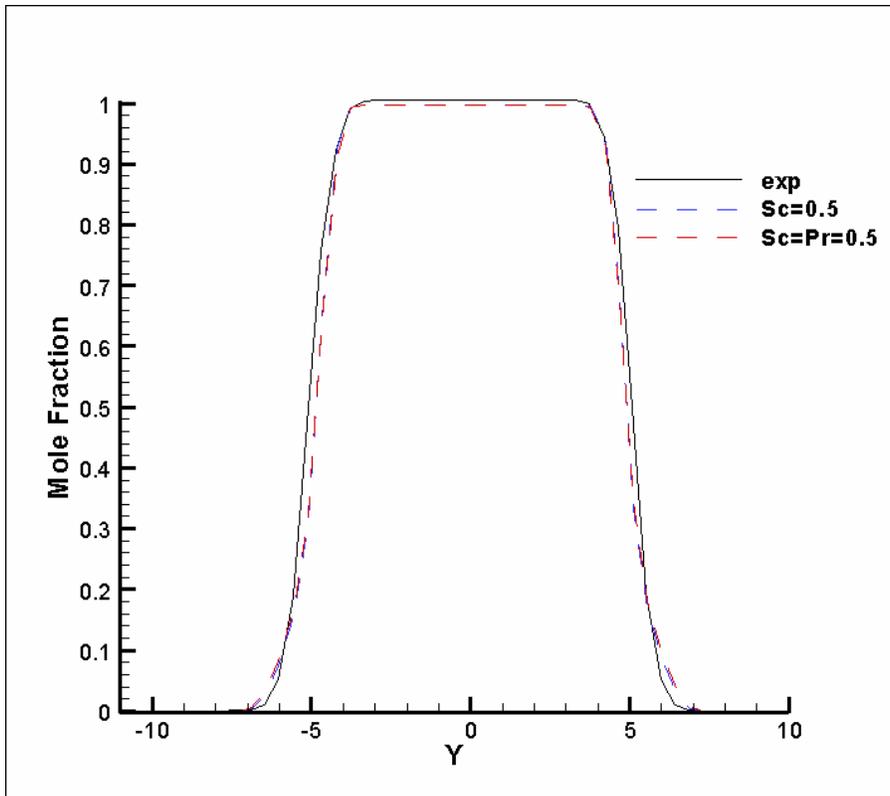
Figure 27   Mole fraction w/ varying Prandtl number Plane 6

A CFD calculation was also done to determine the effect of Pr_t on the flowfield prediction. Figure 27 compares code solutions with $Pr_t = 0.9$ and $Pr_t = 0.5$ (both with $Sc_t = 0.5$) to experimental results at Plane 6 ($x = 43.5$ mm). As the figure shows, the difference is small in Pitot pressure and negligible in the mole fraction.

5.3 Comparisons with He-O$_2$ Data

The CFD case with Sc_t of 0.5 most consistently and accurately predicts the experimental results, and this calculation is plotted with the experimental data for a few survey planes. In figures 28 and 29, there is very good agreement between the argon measurements and calculated results from the nozzle exit until Plane 11 ($x = 162$ mm). This is similar to the outcome of the He-O$_2$ experiment as seen in figures 11 and 30. However, the agreement between the argon data and CFD from Plane 14 ($x = 261$mm) downstream is poor.
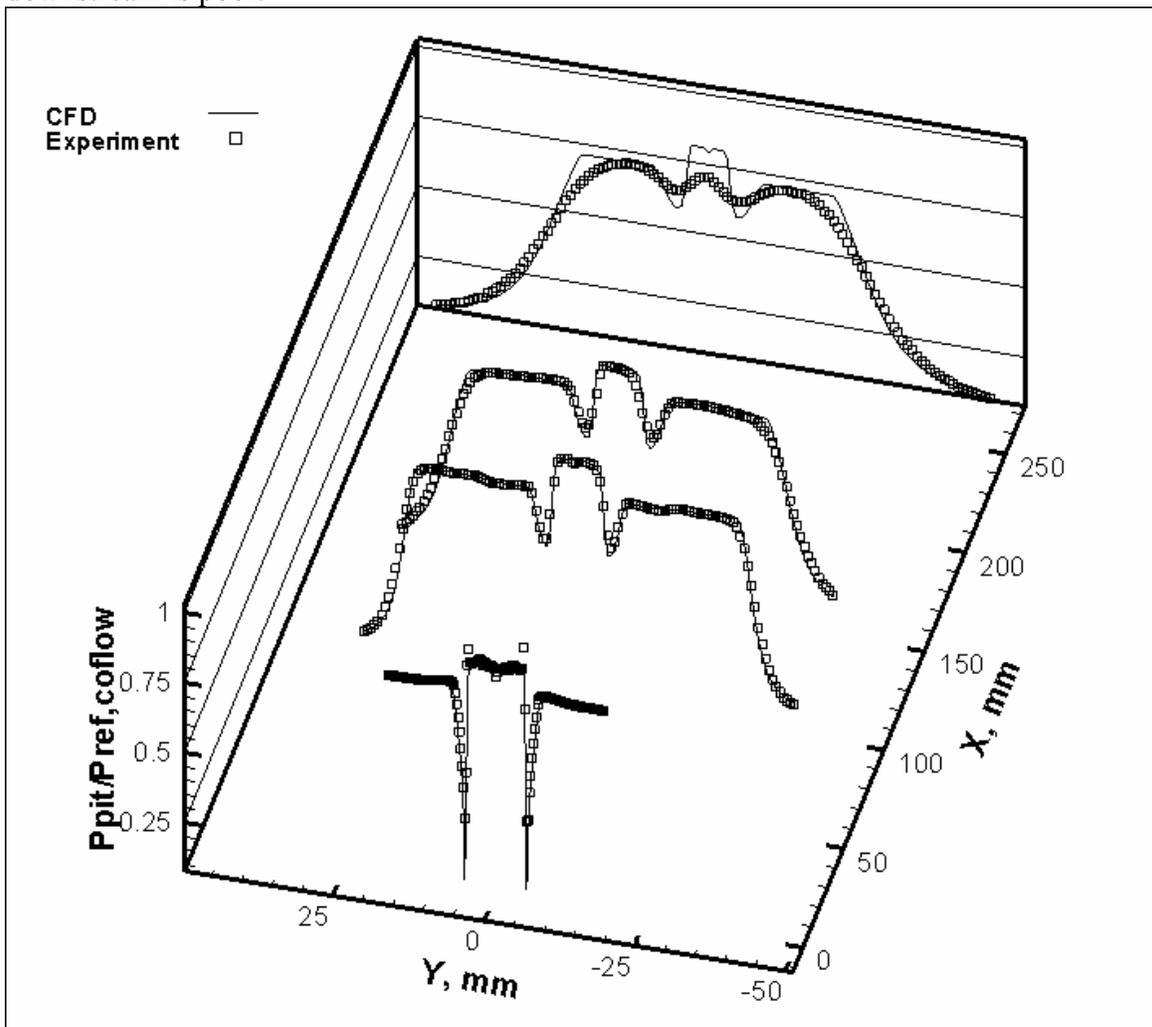

Figure 28   Comparison of argon Pitot pressure measurements with CFD

In both the argon and He-O$_2$ cases, the code underpredicts the mixing in Plane 14 (x = 261 mm). In figure 11, the underpredicted mixing of the coflow is visible in the "shoulders" of the plots of Pitot pressure, but the center jet mixing of He-O$_2$ is reasonably represented by the code. In the argon case, the mixing throughout the entire stream, including that in the core, is underpredicted as shown in figure 28.
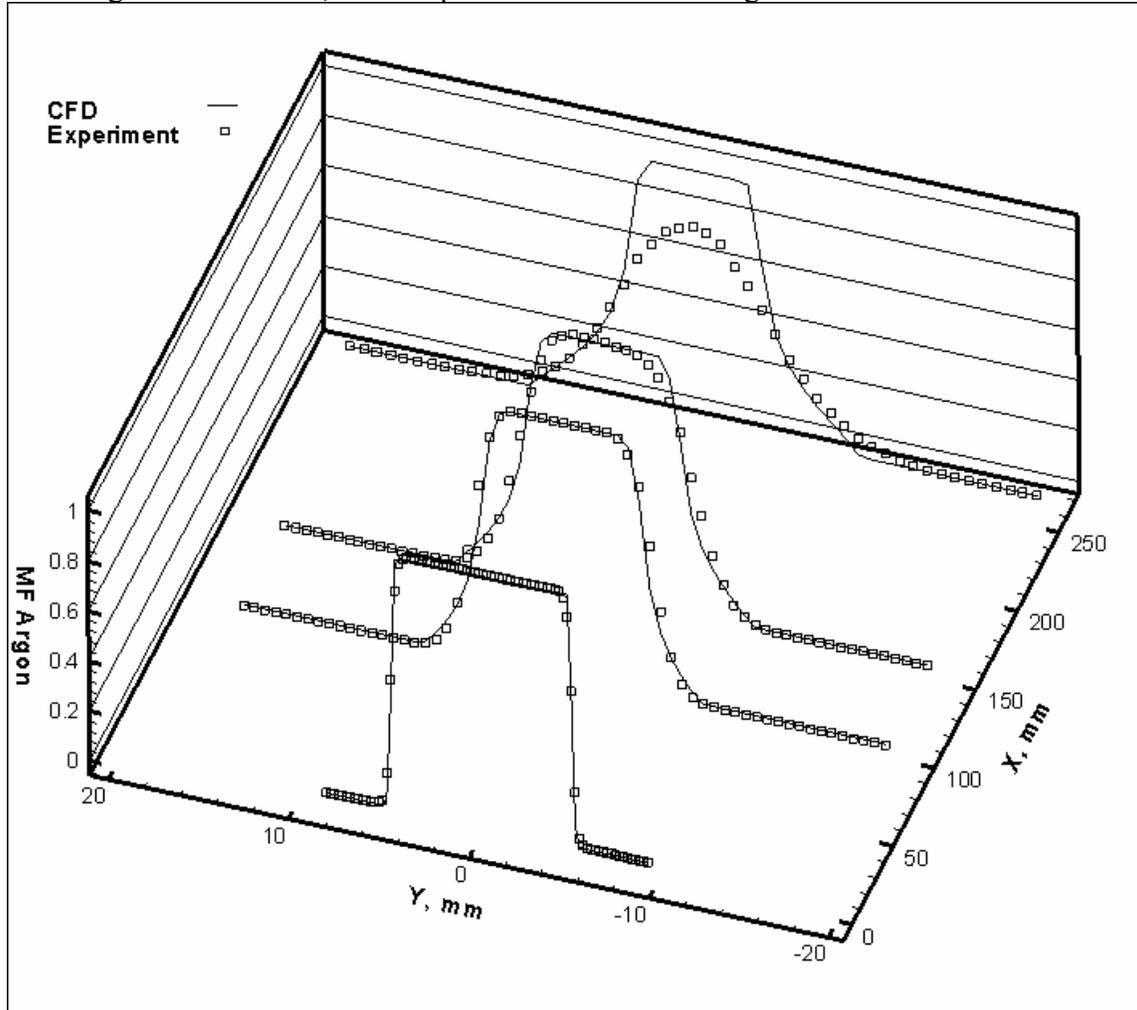
**Figure 29   Comparison of argon mole fraction measurements with CFD**
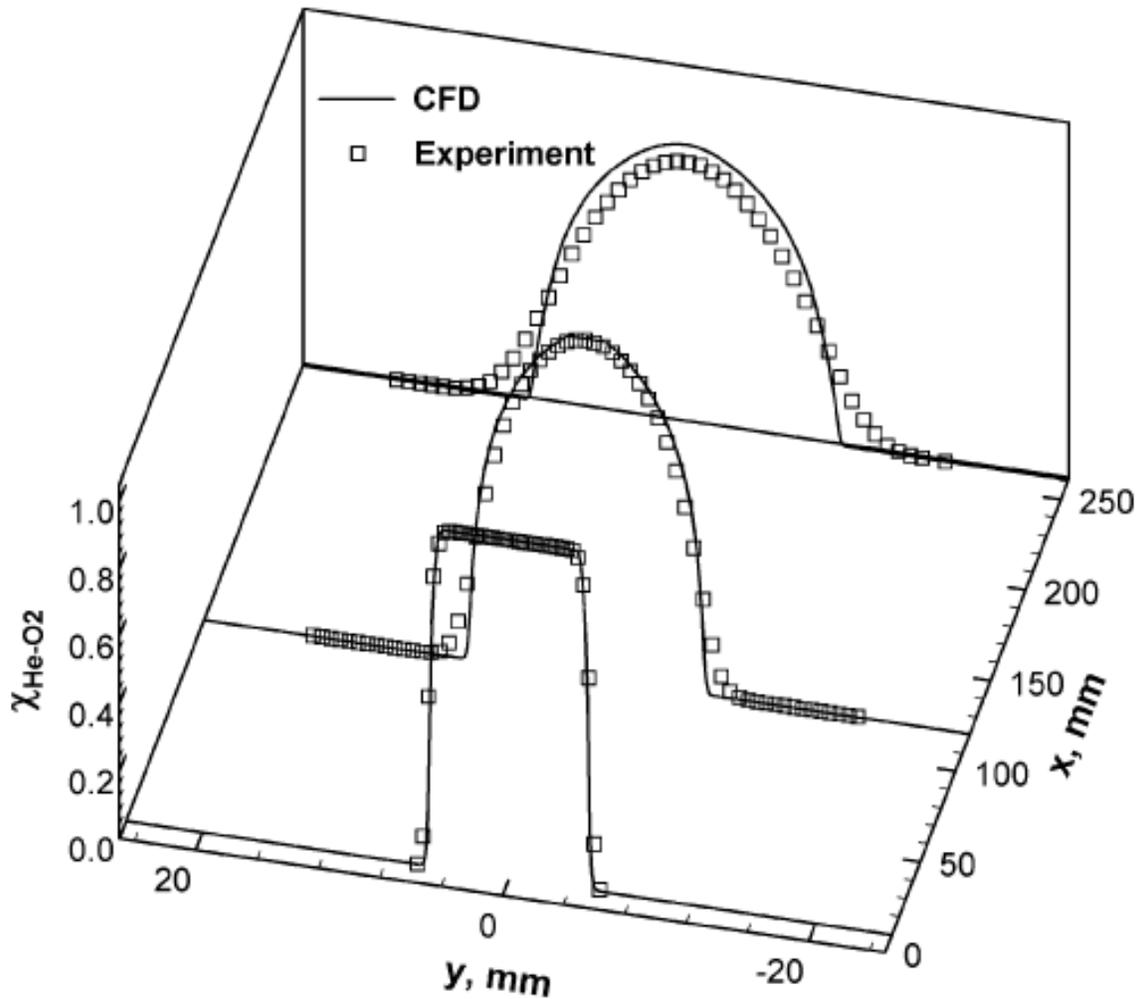
Figure 30   Comparison of He-O$_2$ mole fraction measurements with CFD, from Cutler *et al*.[14]

The boundaries of the mixing layer, defined as the lines where the mole fraction of center jet gas is 0.01 or is 0.99, have been interpolated from the data and are shown, for both argon and He-O$_2$,[14] in figure 31. The magnitudes of the previously defined mixing-layer boundaries, $\delta_{0.01}$ and $\delta_{0.99}$ are shown together in figure 32 where they are plotted as a function of x. Straight lines have been fit to this plot and their equations are included. The thickness of the mixing layer between the center jet and coflow, upstream of x = 181mm where $\delta_{0.99} > 0$, is defined as $\delta_{0.01}$ - $\delta_{0.99}$. The rate of change of this thickness, or mixing-layer growth rate, is 0.0401. This is higher than the growth rate of 0.0318 calculated from an equation given by Papamoschou and Roshko[2] for the "visual thickness" of a two-dimensional incompressible mixing layer between streams that have the same velocity ratio and density ratio.

35

$$\delta'_{vis,0} = 0.17 \frac{\left[1 - \dfrac{u_2}{u_1}\right]\left[1 + \left(\dfrac{\rho_2}{\rho_1}\right)^{\frac{1}{2}}\right]}{1 + \dfrac{u_2}{u_1}\left(\dfrac{\rho_2}{\rho_1}\right)^{\frac{1}{2}}}, \tag{5.1}$$

where subscripts 1 and 2 refer to the higher velocity and lower velocity stream, respectively. The measured He-O$_2$ growth rate, where $M_{c,He} = 0.71$, is significantly less than the incompressible growth rate for He-O$_2$, the ratio of the two being 0.43.[14] This is consistent with previous findings on the effects of compressibility on mixing-layer growth rate such as the equation of Dimotakis[3,4] plotted in figure 33. This plot shows the ratio of compressible mixing-layer growth to incompressible mixing-layer growth rate as a function of M_c, and data from the He-O$_2$ experiment and this experiment have been included for comparison. The measured argon growth rate is relatively close to its calculated counterpart as it should be (although the visual rate, based on schlieren flow visualizations, may not correspond exactly to the rate defined from the Pitot data), the ratio being 1.26. The convective Mach number for the argon mixing case is 0.17 and so the mixing layer between the argon and air is essentially incompressible.
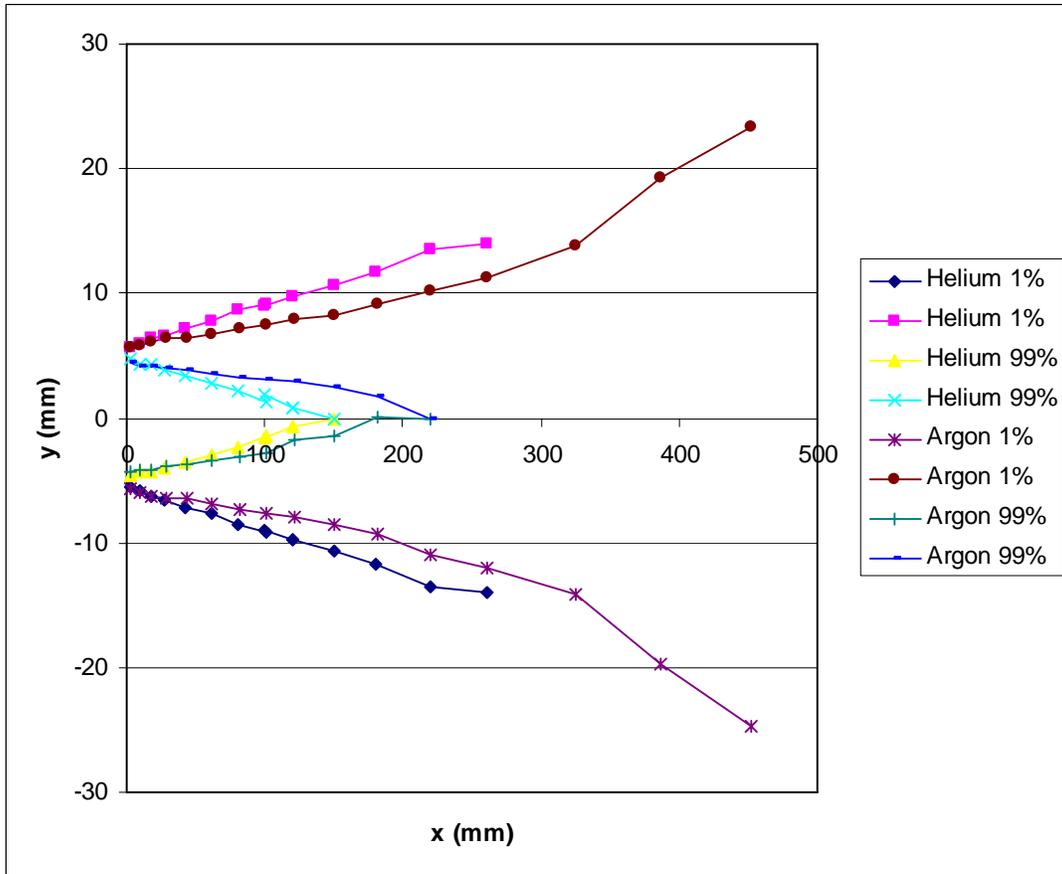

Figure 31   *y*-location of 1% and 99% mole fraction of center jet gas for argon and He-O$_2$ experiments as a function of streamwise distance
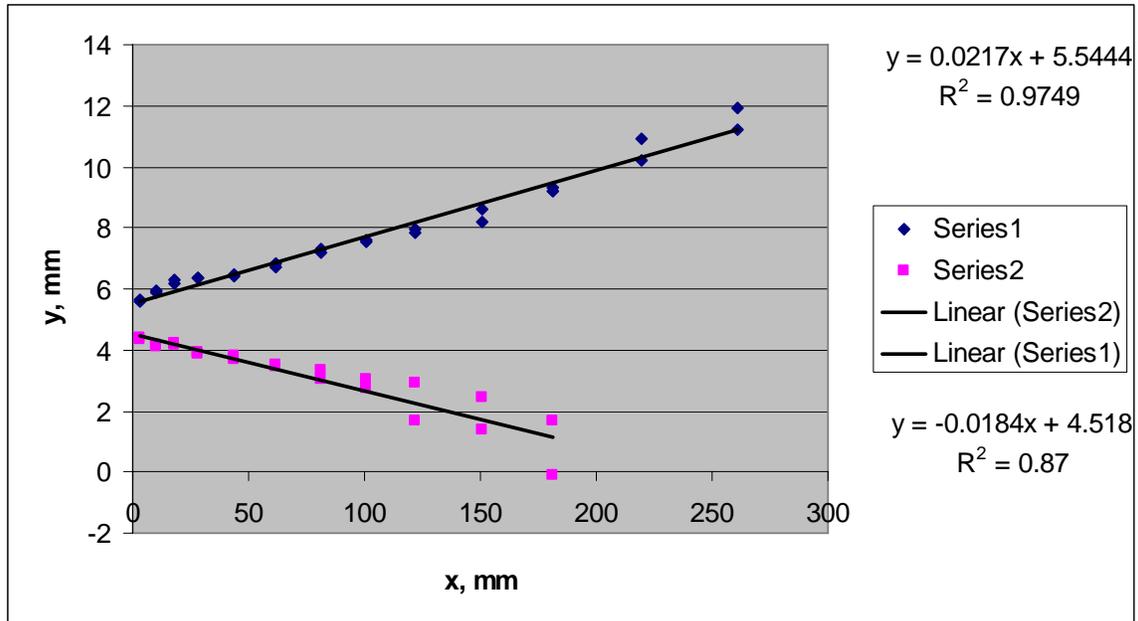
Figure 32   **Magnitude of *y*-location of 1% and 99% mole fraction of center jet gas for argon experiment**
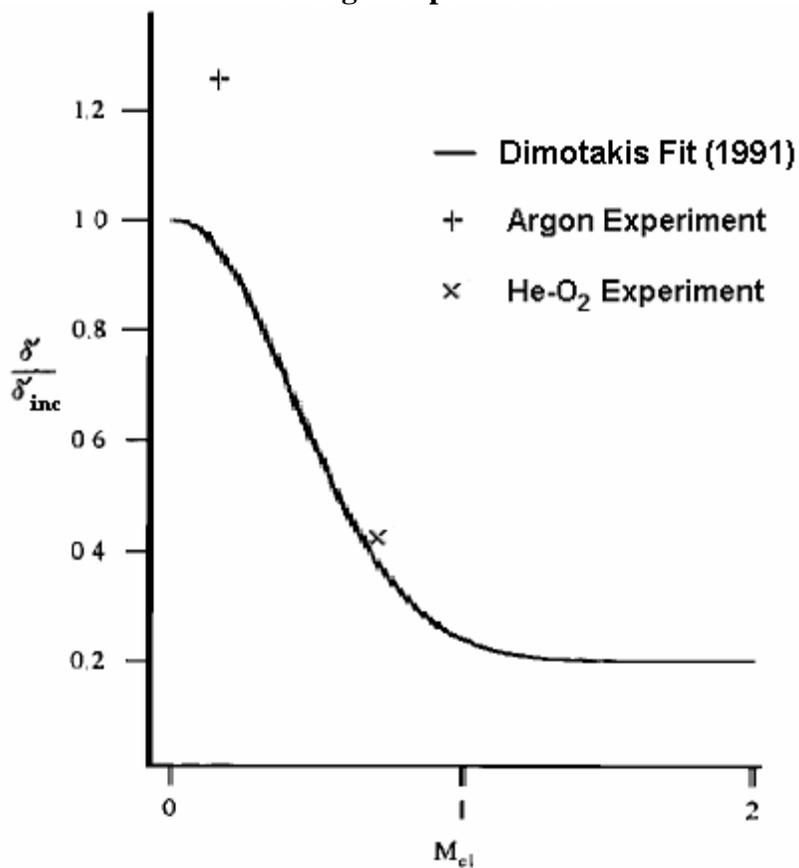

Figure 33   **Ratio of compressible mixing-layer growth to incompressible mixing-layer growth as a function of convective Mach number, modified from Rossmann *et al.*[4]**

5.4 Data Symmetry

In previous figures there is a noticeable lack of symmetry in the argon jet data far downstream of the nozzle exit, presumably caused by a slight misalignment of the center jet. For instance, in figures 25 and 26 the center jet is skewed towards the positive y and in figure 31 the line representing $\chi_{Ar} = 0.99$ on the - y side of the center jet does not mirror the + y, and appears to end prematurely. The cause of this misalignment is unknown as it does not seem to have been present during the experiment of Cutler *et al.*[14]

CHAPTER 6 – CONCLUSION

This paper describes an experiment to acquire data for the validation and development of CFD codes and their turbulence models. A supersonic circular jet of argon was discharged within a concentric, supersonic coflow jet of air. Both nozzle-exit flows open and were a $M = 1.8$ with a static pressure of 1 atm. The M_c of the compressible mixing layer was 0.17, quite small due to the nearly identical sonic speeds associated with each stream. Measurements were taken at the exit plane, as well as at sixteen downstream planes to characterize the flowfield. There was difficulty in obtaining gas composition measurements as accurately as in previous experiments implementing the same probe and apparatus (though different gas mixtures); however, the uncertainty in mole fraction was below 1%. The flowfield development of this experiment was compared to that of a previous experiment in which an He-O_2 mixture was used (in place of argon) in the center jet of the same coaxial jet assembly. These experiments also shared the same facility and data acquisition system, instrumentation, and procedure. The flowfield development (i.e. mixing-layer growth and shock wave propagation) closely resembled one another, although the mixing of argon and air was slower than that of the He-O_2 mixture.

CFD calculations were made using a structured finite-volume code employing Wilcox's k-omega model, and then compared with the measured flowfield. The code was executed with different constant values of Sc_t while holding $Pr_t = 0.9$. These calculations were carried out with, and without, the Pope correction, which is often used to correct round jet mixing-rate predictions of turbulence models. A value of 0.5 for Sc_t was found to best predict the experiment without the Pope correction. There was good agreement between the coaxial argon data and CFD from the nozzle exit throughout most of the measured flowfield (throughout $x = 162$ mm). However, the predicted mixing was significantly less than that found in the experiment in the measured planes further downstream, and the overall agreement between the argon data and calculations was worse than that in the He-O_2 experiment. Significant disagreement was also found in the comparison of experimental and calculated total temperature within the center jet, suggesting an as yet unexplained difference between the CFD and actual experimental argon tank temperatures. Additionally, the argon flowfield data did not maintain symmetry in the downstream planes. This is likely a result of the center jet being slightly misaligned with the coflow.

The argon data are consistent with incompressible mixing-layer growth rates predicted by simple correlations from previous research, although the CFD analysis had more difficulty simulating this flow than the compressible mixing-layer of the He-O_2 experiment. This study indicates that the k-omega turbulence model, which models the Reynolds stress, does not properly predict the mixing rates. Turbulent Schmidt and Prandtl numbers are ratios respectively of the Reynolds stress to mass flux and energy flux; correct prediction of mass and energy fluxes depends also on the accurate prediction of the Reynolds stress.

The data set collected in this experiment complements the previously mentioned He-O$_2$ mixture experiment, and examines a significantly different mixing-layer convective Mach number. The combination of these experiments offers a more complete, and convincing, case for improving high-speed CFD codes than either experiment does alone. Also, this data set, particularly when combined with the data from the He-O$_2$ mixture experiment, is a valuable addition to the growing collection of supersonic mixing data. It provides flowfield data of a supersonic, low M_c mixing-layer of axisymmetric geometry, whereas most of the fundamental studies are of supersonic mixing data in a planar geometry.

REFERENCES

[1] Baurle, R. A., "Modeling of High Speed Reacting Flows: Established Practices and Future Challenges," Paper No. AIAA 2004-267, 42nd Aerospace Sciences Meeting and Exhibit, Reno, NV, Jan 5-8, 2004.

[2] Papamoschou, D., Roshko, A., "The Compressible Turbulent Shear Layer: an Experimental Study," *Journal of Fluid Mechanics*, Vol. 197, 1988, pp. 453-477.

[3] Rossman, T., Mungal, M., Hanson, R., "Evolution and Growth of Large-Scale Structures in High Compressibility Mixing Layers," *Journal of Turbulence*, Vol. 3, No 9, 2002, pp. 1-19.

[4] Rossman, T., Mungal, M., Hanson, R., "A New Shock Tunnel Facility for High Compressibility Mixing Layer Studies," Paper No. AIAA 99-0415, 37th Aerospace Sciences Meeting and Exhibit, Reno, NV, Jan 11-14, 1999.

[5] Davidenko, D., Dufour, E., Magre, P., "Numerical Modeling of Inert and Reacting Compressible Turbulent Jets," Paper No. AIAA 2005-3237, 13th International Space Planes and Hypersonic Systems and Technologies Conference, Capua, Italy, May 16-20, 2005.

[6] Hassan, H. A., Xiao, X., Baurle, R. A., "Modeling Scramjet Flows with Variable Turbulent Prandtl and Schmidt Numbers," Paper No. AIAA 2006-128, 44th Aerospace Sciences Meeting and Exhibit, Reno, NV, Jan 9-12, 2006.

[7] Hassan, H. A., Xiao, X., Edwards, J. R., Cutler, A. D., "Variable Turbulent Schmidt-Number Formulation for Scramjet Applications," Paper No. AIAA 2005-1099, 43rd Aerospace Sciences Meeting and Exhibit, Reno, NV, Jan 10-13, 2005.

[8] Brinckman, K. W., Calhoon Jr, W. H., Tomes, J., Mattick, S. J., Dash, S. M., "Scalar Fluctuation and Transport Modeling for Application to High Speed Reacting Flows," Paper No. AIAA 2006-1452, 44th Aerospace Sciences Meeting and Exhibit, Reno, NV, Jan 9-12, 2006

[9] Brinckman, K. W., Kenzakowski, D. C., Dash, S. M., "Progress in Practical Scalar Fluctuation Modeling for High-Speed Aeropropulsive Flows," Paper No. AIAA 2005-508, 43rd Aerospace Sciences Meeting and Exhibit, Reno, NV, Jan 10-13, 2005.

[10] Brinckman, K. W., Dash, S. M., Kannepalli, C., Ott, J. D., "Scramjet Propulsive Flowpath Prediction Improvements Using Recent Modeling Upgrades," Paper No. AIAA 2005-432, 43rd Aerospace Sciences Meeting and Exhibit, Reno, NV, Jan 10-13, 2005.

[11] Brinckman, K. W., Calhoon Jr, W. H., Tomes, J., Mattick, S. J., Dash, S. M., "Scalar Variance Model Validation for High-Speed Variable Composition Flows," Paper No. AIAA 2006-715, 44th Aerospace Sciences Meeting and Exhibit, Reno, NV, Jan 9-12, 2006.

[12] Hassan, H. A., Xiao, X., Edwards, J. R., Gaffney, R. L., "Role of Turbulent Prandtl Number on Heat Flux at Hypersonic Mach Numbers," Paper No. AIAA 2005-1098, 43rd Aerospace Sciences Meeting and Exhibit, Reno, NV, Jan 10-13, 2005.

[13] Hassan, H. A., Xiao, X., Keistler, P. G., Gaffney, R. L., "Turbulence Modeling for Scramjet Applications," Paper No. AIAA 2005-5382, 35th Fluid Dynamics Conference and Exhibit, Toronto, Canada, Jun 6-9, 2005

[14] Cutler, A. D., White, J. A., Diskin, G. S., Drummond, J. P., "An Experimental and CFD Study of a Supersonic Coaxial Jet," *AIAA Journal*, Vol. 44, No. 3, March 2006, pp. 585-592.

[15] Miles, R. B., Grinstead, J., Kohl, R. H., Diskin, G. S., "The RELIEF Flow Tagging Technique and Its Application in Engine Testing Facilities and for Helium-Air Mixing Studies," *Measurement Science Technologies*, Vol. 11, 2000, pp. 1272-1281.

[16] Doehner, S., "Effects of Jet Swirl on Mixing of a Light Gas Jet in a Supersonic Airstream," M.S. Thesis, SEAS, The George Washington University, 1999.

[17] Omega Engineering, Inc., 2006, http://www.omega.com/toc_asp/frameset.html?book=Temperature&file=TC_GEN_SPECS_REF, "site accessed on 11/21/06."

[18] Bryer, D. W., Pankhurst, R. C., *Pressure-Probe Methods for Determining Wind Speed and Flow Direction*, HMSO, London, 1971.

[19] Cutler, A. D., Johnson, C. H., "Analysis of Intermittency and Probe Data in a Supersonic Flow with Injection," *Experiments in Fluids*, No 23, 1997, pp. 38-47.

[20] Johnson, C., "Applications of Streamwise Vorticity in Enhancement of Injectant Mixing and Penetration in a Supersonic Flow," M.S. Thesis, SEAS, The George Washington University, May 1996.

[21] Ninneman, T. A., Ng, W. F., "A Concentration Probe for the Study of Mixing in Supersonic Shear Flows," *Experiments in Fluids*, No. 13, 1992, pp. 98-104.

[22] Wilcox, D.C., *Turbulence Modeling for CFD*, DCW Industries, Inc., 2nd edition, 1998.

[23] NASA Langley Research Center, 2007, http://vulcan-cfd.larc.nasa.gov/WebPage_manual/vulcan_manual_nsmain.html, "site accessed on 1/22/07."

1. REPORT DATE *(DD-MM-YYYY)* 01- 04 - 2007	2. REPORT TYPE Contractor Report	3. DATES COVERED *(From - To)*

4. TITLE AND SUBTITLE	5a. CONTRACT NUMBER
A Supersonic Argon/Air Coaxial Jet Experiment for Computational Fluid Dynamics Code Validation	
	5b. GRANT NUMBER
	5c. PROGRAM ELEMENT NUMBER

6. AUTHOR(S)	5d. PROJECT NUMBER NNL06AA07A
Clifton, Chandler W.; and Cutler, Andrew D.	5e. TASK NUMBER
	5f. WORK UNIT NUMBER 599489.02.07.07.03.02

7. PERFORMING ORGANIZATION NAME(S) AND ADDRESS(ES)	8. PERFORMING ORGANIZATION REPORT NUMBER
NASA Langley Research Center Hampton, VA 23681-2199 The George Washington University 1 Old Oyster Point Newport News, VA 23602	

9. SPONSORING/MONITORING AGENCY NAME(S) AND ADDRESS(ES)	10. SPONSOR/MONITOR'S ACRONYM(S)
National Aeronautics and Space Administration Washington, DC 20546-0001	NASA
	11. SPONSOR/MONITOR'S REPORT NUMBER(S) NASA/CR-2007-214866

12. DISTRIBUTION/AVAILABILITY STATEMENT
Unclassified - Unlimited Subject Category 34 Availability: NASA CASI (301) 621-0390

13. SUPPLEMENTARY NOTES
Langley Technical Monitor: Aaron H. Auslender An electronic version can be found at http://ntrs.nasa.gov

14. ABSTRACT

A non-reacting experiment is described in which data has been acquired for the validation of CFD codes used to design high-speed air-breathing engines. A coaxial jet-nozzle has been designed to produce pressure-matched exit flows of Mach 1.8 at 1 atm in both a center jet of argon and a coflow jet of air, creating a supersonic, incompressible mixing layer. The flowfield was surveyed using total temperature, gas composition, and Pitot probes. The data set was compared to CFD code predictions made using Vulcan, a structured grid Navier-Stokes code, as well as to data from a previous experiment in which a He-O2 mixture was used instead of argon in the center jet of the same coaxial jet assembly. Comparison of experimental data from the argon flowfield and its computational prediction shows that the CFD produces an accurate solution for most of the measured flowfield. However, the CFD prediction deviates from the experimental data in the region downstream of $x/D = 4$, underpredicting the mixing-layer growth rate.

15. SUBJECT TERMS
Fluid mechanics; Experiments; Gas dynamics; Supersonic mixing; Supersonic shear layers; Supersonic jets; Scramjets; CFD validation

16. SECURITY CLASSIFICATION OF:			17. LIMITATION OF ABSTRACT	18. NUMBER OF PAGES	19a. NAME OF RESPONSIBLE PERSON STI Help Desk (email: help@sti.nasa.gov)
a. REPORT	b. ABSTRACT	c. THIS PAGE			19b. TELEPHONE NUMBER *(Include area code)*
U	U	U	UU	52	(301) 621-0390